Environmental Science and Pollution Research (2023) 30:101933–101962
https://doi.org/10.1007/s11356-023-29564-9

REVIEW ARTICLE

Recent advances in sulfidized nanoscale zero-valent iron materials for environmental remediation and challenges

Wenjing Xue[1] · Jun Li[1] · Xinyu Chen[1] · Hongdou Liu[1] · Siqi Wen[1] · Xiaoyu Shi[1] · Jiaming Guo[1] · Yang Gao[2] · Jian Xu[1] · Yiqun Xu[1]

Received: 14 June 2023 / Accepted: 24 August 2023 / Published online: 2 September 2023

Abstract

Over the past decade, sulfidized nanoscale zero-valent iron (S-nZVI) has been developed as a promising tool for the remediation of contaminated soil, sediment, and water. Although most studies have focused on applying S-nZVI for clean-up purposes, there is still a lack of systematic summary and discussion from its synthesis, application, to toxicity assessment. This review firstly summarized and compared the properties of S-nZVI synthesized from one-step and two-step synthesis methods, and the modification protocols for obtaining better stability and reactivity. In the context of environmental remediation, this review outlined an update on the latest development of S-nZVI for removal of heavy metals, organic pollutants, antibiotic resistance genes (ARGs), and antibiotic resistant bacteria (ARB) and also discussed the underlying removal mechanisms. Environmental factors affecting the remediation performance of S-nZVI (e.g., humic acid, coexisting ions, S/Fe molar ratio, pH, and oxygen condition) were highlighted. Besides, the application potential of S-nZVI in advanced oxidation processes (AOP), especially in activating persulfate, was also evaluated. The toxicity impacts of S-nZVI on the environmental microorganism were described. Finally, the future challenges and remaining restrains to be resolved for better applicability of S-nZVI are also proposed. This review could provide guidance for the environmental remediation with S-nZVI-based technology from theoretical basis and practical perspectives.

Keywords Sulfidized nanoscale zero-valent iron · Heavy metals · Organic pollutants · Environmental factors · Persulfate activation

Introduction

As a result of massive waste discharge and improper treatment, the environmental pollution problem is increasingly serious (Cheng et al. 2023). Among the most detected pollutants, heavy metals (Fan et al. 2013), chlorinated organic pollutants (Gu et al. 2017), antibiotics (Liu et al. 2018), antibiotic resistance genes (ARGs) (Li et al. 2021c), and antibiotic resistant bacteria (ARB) (Wang et al. 2020b) are typical and also cause great damage to human health due to their toxicity and bioaccumulation (Sredlova and Cajthaml 2021). Therefore, an effective strategy is urgently needed to meet the challenges of these pollution problems.

Iron-based nanoparticles have gained popularity as remediation agents to address environmental pollution issues as a result of the advance of environmental nanotechnology (Fan et al. 2017; Zhao et al. 2016). Nanoscale zero-valent iron (nZVI), which is composed of Fe(0) inner core and iron oxide shell, is an environmentally friendly material with high specific surface area, robust reducing capacity, excellent reactivity, abundance, and easy to obtain (Bae et al. 2018). It was demonstrated that nZVI displayed excellent removal effect on heavy metals, organic pollutants, and others and had been widely used in wastewater treatment, groundwater, soil, and sediment remediation (Huang et al. 2016; Li et al. 2022a; Wei et al. 2018). However, unfavorable factors of nZVI such as easy oxidation, agglomeration, and poor electron selectivity limit its large-scale application (Su et al.

Responsible Editor: George Z. Kyzas

✉ Yiqun Xu
qunxyq@163.com

[1] College of Environmental Science and Engineering, Yangzhou University, Yangzhou 225009, China

[2] School of Hydraulic and Environmental Engineering, Changsha University of Science & Technology, Changsha 410114, China

2020). Therefore, a series of modification methods were proposed to address the bottleneck issues and strengthen the performance of nZVI, mainly including doping with noble metals (He et al. 2018), loading on polyporous supporters (Zhu et al. 2017), coating with polymers, and sulfidation (Kong et al. 2021). In comparison with nZVI, sulfidation has gained great research interest due to its multiple superiorities, such as improved the sequestration of pollutants (Du et al. 2016), enhanced reactivity to pollutant transformation (Su et al. 2018), increased selectivity and longevity (Brumovský et al. 2020; Zhu et al. 2021), and reduced aggregation (Garcia et al. 2020b). Compared with most nanomaterials, the nZVI has advantages because of its low cost, eco-friendliness, and high reactivity, and when it is modified with sulfide, it can largely enhance the efficacy and applicability (Crane and Scott 2012). The excellent performance of S-nZVI should be ascribed to the unique core–shell structure, which could provide prominent adsorption and reducing capacity (Wu et al. 2018; Zhu et al 2021). Meanwhile, it was also found that S-nZVI has higher TCE dichlorination efficiency bimetallic nZVI, loading modified nZVI and coating stabilized nZVI, which was caused by the higher electron efficiency and lower hydrogen evolution reaction (Gao et al. 2022b; He et al. 2018; Xu et al. 2020e). Therefore, S-nZVI was a promising amendment agent for environmental remediation. The sulfidation of nZVI, which can be characterized as chemical alteration of nZVI by adding sulfur compounds, produces hydrophobic iron sulfides (e.g., FeS_x) on the surface (Li et al. 2017b). Currently, the most widely used synthesis methods of sulfidized nZVI (S-nZVI) mainly include one-step synthesis and two-step synthesis (Bhattacharjee and Ghoshal 2018a; Xu et al. 2019c). The difference between two synthesis methods lies in the time points at which the iron species are reduced. However, little attention has been paid to the difference between S-nZVI synthesized using these two preparation methods in terms of the composition of surface elements, morphology, and characteristics. Therefore, this paper first summarizes the impacts of various synthesis methods on the physicochemical properties of S-nZVI. Moreover, due to its hydrophobic, magnetic, and nanocharacteristics, S-nZVI particles still have an agglomeration phenomenon (Gong et al. 2020). To solve this problem, some modification measures have been proposed. For instance, Zhang et al. (2019a) reported that S-nZVI loaded on biochar (S-nZVI@BC) performed higher reduction efficiency for nitrobenzene (NB) compared with bare S-nZVI; the reason was that the addition of BC not only enhanced the electron shuttle of S-nZVI, but also increased its adsorption capacity for NB. Li et al. (2021a) demonstrated that S-nZVI coated with alginate polymer accelerated the removal of tetrabromobisphenol A (TBBPA) as well as enhanced the stability of S-nZVI. In light of the existing research, two main modification methods of S-nZVI, including loading onto support materials and coating with polymers, are summarized and discussed.

By now, S-nZVI has already been extensively used for the environmental clean-up of heavy metal and chlorinated organic compound contaminated sites (Garcia et al. 2020a; Lv et al. 2019). Besides, investigations on the elimination of ARGs and ARB by S-nZVI also have attracted increasing attention over the years (Liu et al. 2022c; Yu et al. 2021). However, a systematic evaluation of the interaction mechanisms of S-nZVI towards diverse environmental pollutants is still insufficient. In addition, the decontamination effect of S-nZVI is impacted by a variety of factors in practical application. For example, Lv et al. (2018) observed that the removal of S-nZVI for Cd^{2+} was restrained by the existence of Mg^{2+} and Ca^{2+}, while the presence of Cu^{2+} promoted the Cd^{2+} removal. According to Rajajayavel and Ghoshal (2015), S-nZVI had the best removal efficiency of trichloroethene (TCE) when the S/Fe molar ratio was 0.04–0.08, and the efficiency declined at either higher or lower S/Fe molar ratio. Nevertheless, limited attention has been paid to this issue, and more work is required to assess the factors affecting the application performance of S-nZVI, which is conducive to enhancing the removal efficiency of S-nZVI towards diverse pollutants at the field scale.

Additionally, advanced oxidation processes (AOPs) have been employed in the treatment of groundwater and soil polluted by organic pollutants as a viable chemical oxidation method (Ma et al. 2021; Zhao et al. 2021a). In recent years, persulfate (PS)-based AOP has received intensive attention for the generation of highly oxidative and reactive SO_4^{-}, which could contribute to the elimination of organic pollutants (Chen et al. 2020). nZVI has been reported as an effective source of Fe^{2+} that can activate PS to generate SO_4^{-}. However, there are also some disadvantages for nZVI, especially when nZVI corrodes and produces an excess of Fe^{2+} (Kang et al. 2018a). Compared with nZVI, S-nZVI may be an ideal choice for the activation of PS to achieve effective oxidation of organic pollutants. Here, the viability of using S-nZVI to activate oxidants was discussed in this review. Moreover, previous studies have shown that nZVI has certain toxicity to organisms due to its own characteristics (Kotchaplai et al. 2017; Yoon et al. 2018). Little is known about the environmental toxicity of S-nZVI, despite its widespread usage in the removal of pollutants. Considering the similar characteristics of S-nZVI and nZVI and their release into the environment is inevitable, hence, it is very important to evaluate their toxicity.

By consulting the existing literature, it was found that the current review mainly focuses on the preparation process and characterization of S-(n)ZVI particles as well as the removal of heavy metals and chlorinated organics from water (Fan et al. 2017; Li et al. 2017b). Considering the significant advances in S-nZVI materials in recent years and the

still vacancy of summarizing this material, a comprehensive review on S-nZVI material is vital for accelerating further developments. Therefore, the goals of this review are to (1) introduce different synthesis and modification methods of S-nZVI materials; (2) summarize the application of S-nZVI in elimination of heavy metals, organic pollutants, ARGs and ARB, and discuss the underlying removal mechanisms; (3) examine the factors influencing the efficacy of S-nZVI in removing pollutants; (4) illustrate the application scenarios and magnificent prospect of S-nZVI coupled AOP in environmental remediation; and (5) assess the ecotoxicity of S-nZVI as well as the alleviative measures. Finally, the prospects and challenges of S-nZVI-based remediation technology are proposed. The structure of this review is illustrated in Fig. 1.

Preparation and modification methods of S-nZVI

Different preparation methods and compositional characteristics of S-nZVI

The terms "S-nZVI$_{One\text{-}step}$" and "S-nZVI$_{Two\text{-}step}$" referred to S-nZVI synthesized using the one-step and the two-step synthesis methods, respectively (Li et al. 2017b). The specific synthesis process for S-nZVI$_{One\text{-}step}$ involved adding sulfur source and reducing agent simultaneously to the solution containing iron species; then, the Fe^{2+} or Fe^{3+} in the solution and the newly generated nZVI particles could react with sulfur species in the existence of strong reductant at the same time, leading to the formation of S-nZVI$_{One\text{-}step}$ (Wang et al. 2020a). Generally, sodium borohydride ($NaBH_4$) was used as a reducing agent, and sodium dithionate ($Na_2S_2O_4$), sodium sulfide (Na_2S), and sodium thiosulfate ($Na_2S_2O_3$) served as the sulfur sources for the synthesis of S-nZVI (Han and Yan 2016). Kim et al. (2011) proposed a novel and facile method to synthesize S-nZVI for the first time, in which a proper amount of $Na_2S_2O_4$ and $NaBH_4$ was mixed and added dropwise to the Fe^{3+} solution. The two-step synthesis method was namely producing nZVI via liquid-phase reduction method, then adding sulfur source to sulfurize nZVI under certain situations (Xu et al. 2019b). For example, Rajajayavel and Ghoshal (2015) added the $NaBH_4$ solution dropwise into the $FeSO_4{\cdot}7H_2O$ solution to synthesize nZVI, then sulfurized the prepared nZVI with Na_2S solution through ultrasonic treatment to form S-nZVI$_{Two\text{-}step}$. The schematic diagram for the preparation of S-nZVI$_{One\text{-}step}$ and S-nZVI$_{Two\text{-}step}$ is presented in Fig. 2.

The sulfur species distribution of S-nZVI$_{One\text{-}step}$ is different from that of S-nZVI$_{Two\text{-}step}$, in which Fe_xS_y is formed on the pre-synthesized nZVI particles, and Fe^0 and Fe_xS_y of the two-step method are formed in a separate step (Fig. 2). The inner core of S-nZVI$_{One\text{-}step}$ is enriched in sulfur species, whereas only a few parts are uniformly distributed on the surface (Su et al. 2018). The surface is mainly the mixed shell of iron (oxyhydr) oxide and Fe_xS_y (Han and Yan 2016; Su et al. 2015). For S-nZVI$_{Two\text{-}step}$, Fe_xS_y precipitation is unevenly distributed on its surface and is composed of multiphase, and sulfur

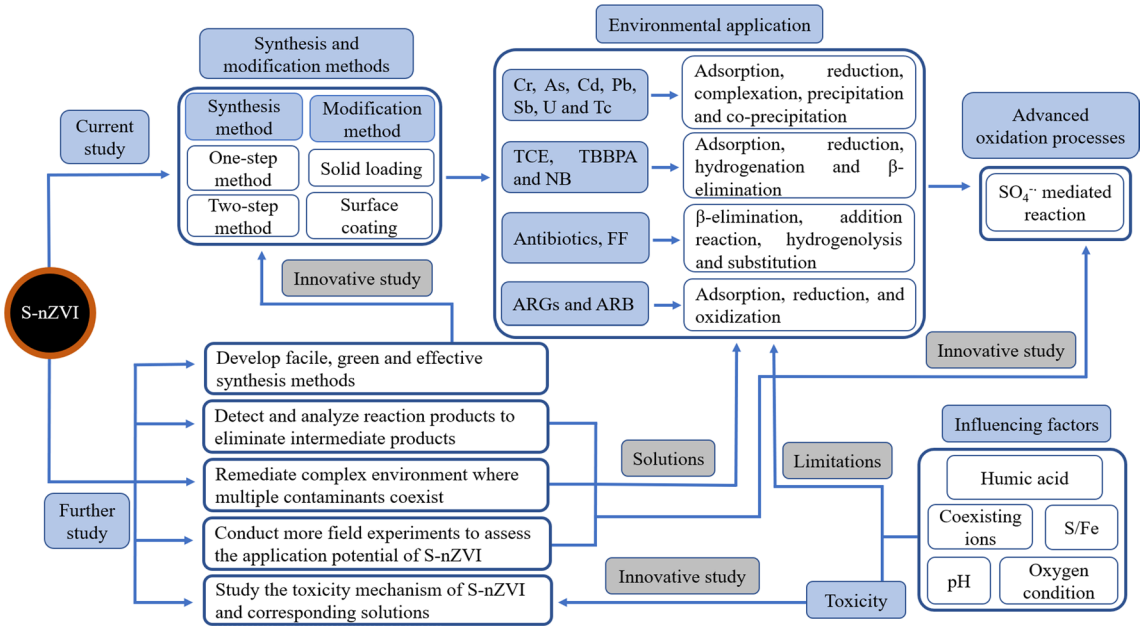

Fig. 1 Overview of the review structure

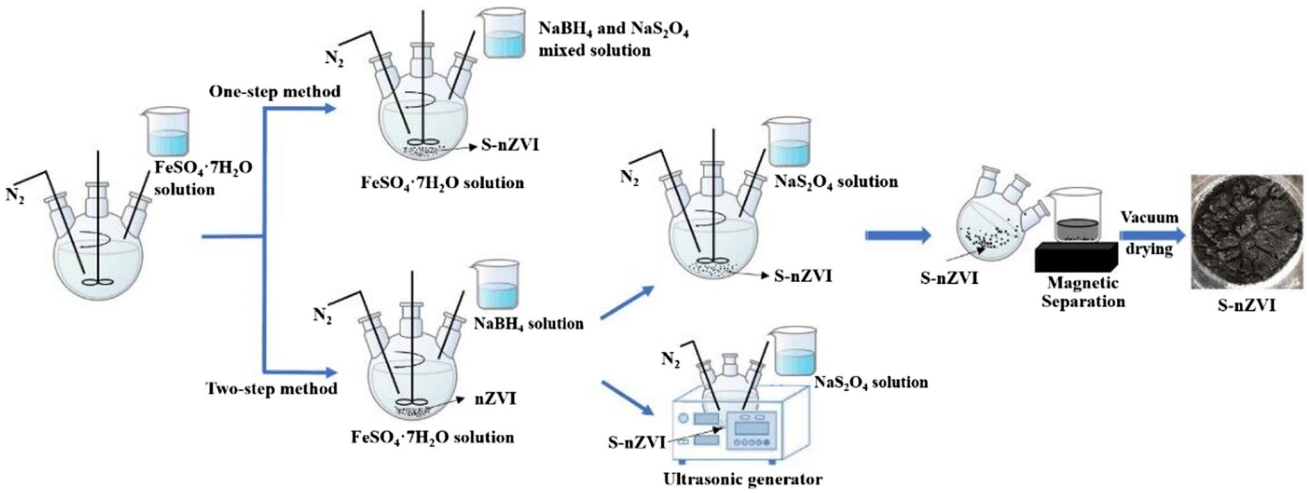

Fig. 2 Schematic diagram for the preparation of S-nZVI$_{One\text{-}step}$ and S-nZVI$_{Two\text{-}step}$ (e.g., $FeSO_4{\cdot}7H_2O$ and $Na_2S_2O_4$)

mainly exists in the form of FeS (Bhattacharjee and Ghoshal 2018a; He et al. 2018). Bhattacharjee and Ghoshal (2018a) reported that FeS existed in the S-nZVI$_{One\text{-}step}$ cores and shells, with small amounts of polysulfides and sulfates in the shells of S-nZVI$_{One\text{-}step}$. In two-step method (S-nZVI$_{Two\text{-}step}$), FeS was mainly distributed on the outer surface, and polysulfides or sulfates were not observed. However, S-nZVI particles were oxidized to different degrees in both one-step and two-step processes. Two works by Xu et al. (2020c) and Xu et al. (2019b) confirmed that FeOOH and $Fe(OH)_2$ were presented on the surfaces of S-nZVI$_{One\text{-}step}$ prepared with $Na_2S_2O_4$, and Fe_2O_3 was the primary oxidized iron species for S-nZVI$_{Two\text{-}step}$ synthesized with Na_2S, respectively. Notably, the impact of the iron precursor on sulfur species distribution of S-nZVI$_{One\text{-}step}$ or S-nZVI$_{Two\text{-}step}$ was not significant, whereas that of the sulfur precursors was marked (Xiao et al. 2022; Xu et al. 2020b). For instance, according to Xu et al. (2020b), FeS_2 was found to be the predominant sulfur species of S-nZVI$_{One\text{-}step}$ made from $Na_2S_2O_4$, while FeS was the dominant sulfur species of S-nZVI$_{One\text{-}step}$ made from Na_2S and K_2S_6. Compared with the latter S-nZVI$_{One\text{-}step}$, the former S-nZVI$_{One\text{-}step}$ had higher hydrophobicity, reactivity, and TCE selectivity. The effect of sulfur sources, including $Na_2S_2O_4$, Na_2S, and $Na_2S_2O_3$, on the efficacy of S-nZVI in a simulated groundwater environment was explored by Xiao et al. (2022). It was observed that the fraction of reducing sulfur species in S-nZVI$_{Two\text{-}step}$ with Na_2S as sulfur agent was higher than that with $Na_2S_2O_3$ or $Na_2S_2O_4$, leading to higher selectivity of S-nZVI$_{Two\text{-}step}$ produced from Na_2S. Hence, sulfur precursors may have a vital and varied impact on the purification ability of S-nZVI under various synthetic situations, which could be chosen to maximize the decontamination performance of S-nZVI in accordance with practical requirements.

From the morphology of particle, S-nZVI$_{One\text{-}step}$ is mainly spherical and contains a small amount of cubic (Fig. 3c) (Xu et al. 2019c), needle, plate-like, and some irregular particles (Fig. 3a1-a4) (Bhattacharjee and Ghoshal 2018a). S-nZVI$_{Two\text{-}step}$ fabricated by Na_2S or $Na_2S_2O_4$ has smooth spherical particles grouped in a representative chain-like pattern (Fig. 3b and d) (Bhattacharjee and Ghoshal 2018a; Xu et al. 2019c), and the particles are surrounded by needle and plate-like configuration (Fig. 3b1) (Bhattacharjee and Ghoshal 2018a). In comparison to the S-nZVI$_{Two\text{-}step}$, the particles of S-nZVI$_{One\text{-}step}$ are more dispersed. And as the S/Fe molar ratio rises, the S-nZVI$_{One\text{-}step}$ particle surface becomes rougher, resulting in larger particle size (Song et al. 2017; Wu et al. 2018). For instance, Wu et al. (2018) evaluated the effect of the presence of $Na_2S_2O_4$, as a sulfur source, on the surface morphology in the synthesis process of S-nZVI$_{One\text{-}step}$. The surface roughness of nanoparticles dramatically strengthened with the S/Fe molar ratio elevating from 0 to 0.35. The specific surface area of S-nZVI$_{One\text{-}step}$ and S-nZVI$_{Two\text{-}step}$ was impacted by the variations in particle size. Generally, S-nZVI$_{One\text{-}step}$ had a comparatively small specific surface area when its particle size was larger. Xu et al. (2019c) confirmed that the specific area of S-nZVI$_{Two\text{-}step}$ (13.8 m^2/g) was 2.2 times larger as compared to that of S-nZVI$_{One\text{-}step}$ (6.4 m^2/g). Also, it was observed that the typical nZVI chain structure in S-nZVI-$_{One\text{-}step}$ was destroyed, which was mainly attributed to the strengthening of steric stability and electrostatic repulsion between S-nZVI particles provided by the plate-like structure (Lv et al. 2018; Song et al. 2017). Accordingly, there are certain differences between S-nZVI$_{One\text{-}step}$ and

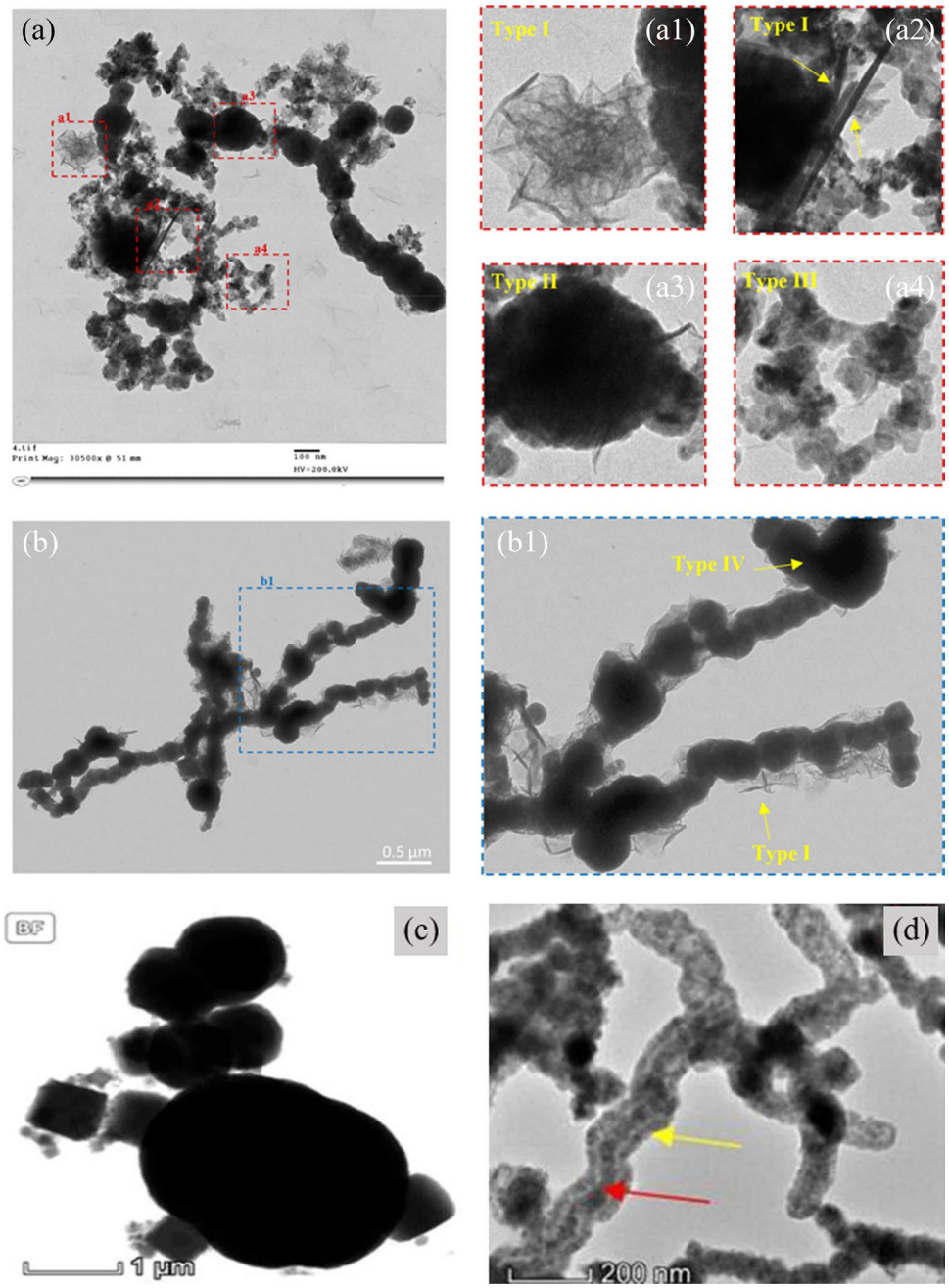

Fig. 3 **a** Representative transmission electron microscopy (TEM) image of S-nZVI$_{One\text{-}step}$. Panels a1–a4 are enlarged images of the dotted boxes area in **a** (type I is needle- and plate-like structures, type II is spherical particles, type III is small irregular particles, and type IV is chain-like spherical structure). **b** Representative TEM image of S-nZVI$_{Two\text{-}step}$. Panel b1 is the enlarged image of the dotted box area in **b**. Reprinted with permission from Ref. (Bhattacharjee and Ghoshal 2018a). Copyright 2018, American Chemical Society; Bright field (BF) TEM images for (**c**) S-nZVI$_{One\text{-}step}$ and (**d**) S-nZVI$_{Two\text{-}step}$. Reprinted with permission from Ref. (Xu et al. 2019c). Copyright 2019, American Chemical Society

S-nZVI$_{Two\text{-}step}$ in the morphology and particle size, and further investigation on how to tune the physicochemical features of S-nZVI via the adjustment of synthesis condition is needed. The physicochemical characteristics of the S-nZVI particles produced using the two synthesis methods are summarized in Table 1.

In addition, it was demonstrated by previous research that S-nZVI$_{One\text{-}step}$ tended to be more selective and reactive than S-nZVI$_{Two\text{-}step}$, which was due to the highest content of Fe^0 and reduced sulfur in S-nZVI$_{One\text{-}step}$ and its stronger electron transfer ability and hydrophobicity (Xiao et al. 2022; Xu et al. 2019c). Xu et al. (2019c) found that S-nZVI$_{One\text{-}step}$ with higher sulfur content provided better hydrophobicity and higher selectivity and reactivity with TCE in comparison with S-nZVI$_{Two\text{-}step}$. However, S-nZVI$_{Two\text{-}step}$ has excellent long-term performance compared to S-nZVI$_{One\text{-}step}$. Xiao et al. (2022) demonstrated that the degradation rate of S-nZVI$_{Two\text{-}step}$ towards TCE remained at 30–60% even after 90 days of aging, while the selectivity of S-nZVI$_{One\text{-}step}$ decreased sharply. Also, it is evident that one-step synthesis method provides more merits and is adaptable for environmental remediation over two-step synthesis method as far as applications are concerned.

Table 1 Effect of different preparation methods on the physicochemical characteristics of S-nZVI

Material	Sulfidation method	Sulfur source and iron source	Size (nm)	Surface area (m^2/g)	Morphology and structure	Sulfur species	S/Fe ratio	References
S-nZVI	One-step	$Na_2S_2O_4$ and $FeCl_3{\cdot}6H_2O$	1000	1.5–12	N.A	S^{2-}, S_2^{2-}, S_n^{2-}, and SO_4^{2-}	0–0.35	(Xu et al. 2020c)
S-nZVI	One-step	$Na_2S_2O_4$ and $FeCl_2{\cdot}4H_2O$	150–200	N.A	Core–shell structure	S^{2-}, S_2^{2-}, S_n^{2-}, and SO_3^{2-}	0.01–0.3	(Mangayayam et al. 2019)
S-nZVI	One-step	$Na_2S_2O_4$ and $FeCl_3{\cdot}6H_2O$	300–2200	6.4	Dominantly spherical particles together with individual cubes	S^{2-}, S_2^{2-}, and S_n^{2-}	0.14	(Xu et al. 2019c)
S-nZVI	One-step	Na_2S and $FeSO_4{\cdot}7H_2O$	100–150	20.26–30.67	Spherical, needle, plate-like, and some irregular particles	S^{2-}, SO_4^{2-}, and polysulfide	0.035–0.4	(Bhattacharjee and Ghoshal 2018a)
S-nZVI	One-step	$Na_2S_2O_4$ and $FeSO_4{\cdot}7H_2O$	150–410	62.5	Aggregated of small spherical particles surrounded by a separate phase of acicular particles	S_n^{2-}, SO_3^{2-}, and SO_4^{2-}	0.035–0.28	(Cao et al. 2017)
S-nZVI	One-step	$Na_2S_2O_4$ and $FeSO_4{\cdot}7H_2O$	200	N.A	Flake-like phase on the shell	S^{2-}, S_2^{2-}, S_n^{2-}, SO_3^{2-}, and SO_4^{2-}	0.07–0.35	(Wu et al. 2018)
S-nZVI	Two-step	Na_2S and commercial nZVI	40–120	15.5–36.7	Irregular spherical shape	S^{2-} and S_2^{2-}	0.0025–0.25	(Brumovský et al. 2020)
S-nZVI	Two-step	Na_2S and $FeCl_3{\cdot}6H_2O$	60–110	13.8	Chain-like aggregates with core–shell structure	S^{2-}, S_2^{2-}, S_n^{2-}, SO_3^{2-}, and SO_4^{2-}	0.14	(Xu et al. 2019c)
S-nZVI	Two-step	Na_2S and $FeCl_3{\cdot}6H_2O$	40–100	5–35	Chain-like structure	S^{2-}, S_2^{2-}, S_n^{2-}, and SO_4^{2-}	0.1–0.5	(Xu et al. 2019b)
S-nZVI	Two-step	Na_2S and $FeCl_3{\cdot}6H_2O$	50–60	N.A	Regular spherical shape	S^{2-}, S_n^{2-}, and SO_4^{2-}	0.3	(Li et al. 2021d)
S-nZVI	Two-step	Na_2S and $FeSO_4{\cdot}7H_2O$	188–200	21–26	N.A	S^{2-} and S_2^{2-}	0.015–1.612	(Rajajayavel and Ghoshal 2015)
S-nZVI	Two-step	Na_2S and $FeCl_3{\cdot}6H_2O$	20–80	N.A	Chain-like aggregates accompanied by a laminar phase	S^{2-}	0–1.12	(Fan et al. 2013)
S-nZVI	Two-step	Na_2S and $FeSO_4{\cdot}7H_2O$	50–200	19.72–21.3	Chain-like spherical structure, needle, and plate-like	S^{2-}	0.035–0.4	(Bhattacharjee and Ghoshal 2018a)

Modifications for improved performance of S-nZVI

Although S-nZVI has been widely used in the removal of a variety of environmental pollutants, the inherent properties of S-nZVI, especially the reactivity and stability, must be further enhanced with the increasing demand. So far, modification of solid supporting and surface coating had been adopted as the main approach to pursue an improvement in the performance of S-nZVI (Garcia et al. 2020b; Jiang et al. 2022; Semerád et al. 2020; Shen et al. 2021; Xu et al. 2022; Zhang et al. 2023). Some common supports and

coating materials are discussed in more detail in the following sections.

Loading S-nZVI onto supports

Modification of solid supporting is usually achieved by choosing the proper carrier firstly, and then, S-nZVI nanoparticles are uniformly dispersed on the surface of the carrier. S-nZVI composites with higher surface area and lower agglomeration can be obtained via solid loading. Some supports with adsorption capacity can further facilitate the contacts between S-nZVI and pollutants, which largely promotes the degradation efficiency (Li et al. 2021b; Zhang et al. 2019b). In a meanwhile, a variety of functional groups (e.g., carboxyl, hydroxyl, and amino) of supports can chelate with S-nZVI, thus enhancing the stability and dispersion of S-nZVI particles (Liu et al. 2020a). Common supporting materials mainly include carbon-based materials (Jiang et al. 2022; Liu et al. 2020a; Zhang et al. 2019b), clay minerals (Chen et al. 2022; Fu et al. 2015; Gao et al. 2022b) and others (Li et al. 2021e; Tan et al. 2022; Zhou et al. 2022).

Carbon-based materials have aroused extensive attention because of their low cost, high surface area, excellent conductivity, and strong adsorption capability (Fu et al. 2023; Harindintwali et al. 2023). Carbon supported-S-nZVI have been synthesized with numerous materials, including BC (Gao et al. 2022a; Xu et al. 2019a, 2021; Zhang et al. 2018), activated carbon (AC) (He et al. 2022; Qu et al. 2021), graphene (Bin et al. 2020; Sun et al. 2020), and carbon nanotubes (CNTs) (Wu et al. 2022b). BC is a kind of environmentally friendly adsorption material derived from diverse biomass waste, and it has the features of high carbon content, excellent pore structure, and various oxygen-containing functional groups (Xu et al. 2021; Zhang et al. 2018). Zhang et al. (2018) synthesized S-nZVI@BC with rice husks as the carbon source and applied it for the removal of NB. Results suggested that the removal efficiency of S-nZVI@BC for NB could reach up to 60% within 10 min, while only 5% of NB was removed with S-nZVI treatment in the same degradation time. The application of BC largely increased the dispersity, adsorption capacity, and antioxidant capacity of S-nZVI. Aiming to further enhance the NB reduction, Zhang et al. (2019a) pretreated BC with HCl, NaOH and H_2O_2, termed as BC/HCl, BC/NaOH, and BC/H_2O_2, respectively. It was demonstrated that the removal efficiencies of NB by S-nZVI@BC/HCl, S-nZVI@BC/NaOH, and S-nZVI@BC/H_2O_2 were 100%, 92.1 ± 4.2%, and 35.2 ± 9.4%, respectively. The excellent removal efficiency of S-nZVI@BC/HCl for NB was attributed to the higher surface area, abundant negative surface charge, and superior electron transfer efficiency. It is also reported that S-nZVI amended with AC possesses great application potential for removal of heavy metals. He et al. (2022) synthesized S-nZVI@AC using sewage sludge for the removal of Cr^{6+}. The reduction capacity of Cr^{6+} by S-nZVI@AC was up to 136.0 mg/g, while that by nZVI sulfurized by Na_2S and $Na_2S_2O_4$ were 66.7 and 65.4 mg/g, respectively. The AC loading significantly expanded the surface area of S-nZVI and effectively lowered its agglomeration, resulting in excellent Cr^{6+} scavenging performance. Recently, it has been found that the hydrophilic treatment can equip AC with some functional groups, such as -OH and -COOH, which increases S-nZVI dispersity in aqueous solution and strengthens the affinity to targeted pollutants. Qu et al. (2021) synthesized hydrophilic porous activated carbon (HPAC) supported S-nZVI (S-nZVI@HPAC) with corn straw as raw material and green tea extracts as reducing reagent for the removal of Pb^{2+} in the water and achieved better removal performance. In addition, it has also been demonstrated that S-nZVI supported by graphene or graphene oxide is superior to the bare S-nZVI for the removal of organic pollutants. According to Bin et al. (2020), the graphene aerogel loading of S-nZVI (S-nZVI/GA) possessed higher electron transport and less agglomeration as compared to S-nZVI. Besides, the GA loading evidently enhanced the TCE removal and complete TCE removal was obtained by S-nZVI/GA within 50 min.

Up to date, clay minerals (e.g., montmorillonite, sepiolite, kaolinite, and attapulgite) have received increasing attention owing to their wide availability, economically friendly, environmental stability, and high adsorption capacities and ion exchange properties (Fan and Tahir 2022; Haciosmanoğlu et al. 2022; Uddin 2017). The physicochemical properties of clay minerals vary with the geographical origin and mineral type, which increases their utilization as adsorbents and enables them to be used as supports. Clay supported S-nZVI composite materials have been developed as effective remedial alternatives relative to bare S-nZVI in recent years (Ezzatahmadi et al. 2017). Montmorillonite is a typical and cost-effective 2: 1 layered silicate clay mineral having excellent adsorption ability and high cation exchange capacity (Xu et al. 2020a). Besides, its layer has permanent negative charges due to the isomorphous substitution within the layer (e.g., the replacement of Al^{3+} by Mg^{2+} and Si^{4+} by Al^{3+}). Therefore, it can attract cations and provide high cation exchange capacity, making it an ideal carrier for S-nZVI (Ezzatahmadi et al. 2017). Accordingly, Xu et al. (2020a) fabricated an S-nZVI-based composite using montmorillonite as the carrier (S-nZVI@MMT) to remove TCE in the groundwater substrate and found that the removal performance of S-nZVI@MMT towards TCE still maintained relatively great even in the existence of high concentration of humic acid or after aging for 30 days. Furthermore, it was observed that the montmorillonite loading remarkably increased the TCE degradation efficiency by S-nZVI, which was caused by the excellent reactivity of S-nZVI clusters forming in the interlayer of MMT. Sepiolite is a kind

of low-cost clay mineral with chemically stable and high adsorption characteristics (Ainiwaer et al. 2022; Daneshkhah et al. 2017; Ezzatahmadi et al. 2017). Fu et al. (2015) prepared a novel composite where sepiolite is a carrier of S-nZVI for the removal of Cr^{6+} and Pb^{2+} in the groundwater. It was demonstrated that the sepiolite supported S-nZVI had larger specific surface area and lower agglomeration tendency as compared to pure S-nZVI. Moreover, S-nZVI loaded with kaolinite and attapulgite had similar characteristics with sepiolite and exhibited effective removal of heavy metals from water (Chen et al. 2022; Gao et al. 2022b). In addition, there are also some other materials serving as supports of S-nZVI and providing good pollutant removal performance, including resin (Zeng et al. 2022), zeolite (Zhou et al. 2021b, 2022), blast furnace slag (BFS) (Deng et al. 2020; Li et al. 2021e; Tan et al. 2022), among others.

Surface coating of S-nZVI

Modification of surface coating is namely applying the polymer coating onto the S-nZVI surface, thus enhancing the stability and dispersity of S-nZVI through the generated electrostatic and spatial repulsive forces. The common polymers include carboxymethyl cellulose (CMC) (Devi and Dalai 2019; Wu et al. 2021; Yu et al. 2020) and alginate (Li et al. 2019; Zhang et al. 2020c). CMC is a synergistic polymer compound, which is also a derivant of cellulose and extensively applied in coating magnetic nanoparticles (Kong et al. 2021; Lefevre et al. 2016). Gong et al. (2020) reported that CMC-S-nZVI displayed better physical stability and mobility in saturated porous media than the unstable S-nZVI. This phenomenon was attributable to stronger spatial repulsion caused by the adsorption of CMC on the surface of the Fe_xS_y coating of S-nZVI. These investigations offer convincing proof that, at the field scale, the restrictions of nZVI or S-nZVI regarding mobility could be effectively addressed by polymer stabilization.

Similar to the synthesis of S-nZVI, two different methods were proposed for the preparation of CMC-S-nZVI due to the different sequence of CMC stabilization and sulfurization (Fig. 4). The dispersion of CMC-S-nZVI$_{One\text{-}step}$ is stronger than that of CMC-S-nZVI$_{Two\text{-}step}$, possibly due to the lower sulfur content for nZVI because CMC can peel off the FeS shell in the two-step method. The Na^+ of the sulfiding agent and the Fe^{2+} dissolved from the FeS precipitate reduce the CMC viscosity, resulting in accelerated deposition and reduced mobility of the nZVI (Kong et al. 2021; Xu et al. 2020e). Kong et al. (2021) found that the variation of CMC modified sequence could lead to significant differences in the resulting CMC-S-nZVI composites. Specifically, the CMC-S-nZVI$_{Two\text{-}step}$ provided better reactivity and electron selectivity, while the composite produced by CMC-S-nZVI$_{One\text{-}step}$ displayed higher mobility. For the morphology of CMC-S-nZVI$_{One\text{-}step}$ and CMC-S-nZVI$_{Two\text{-}step}$, Xu et al. (2020e) found that both sulfuration methods produced particles with distinguishable core–shell structure. By comparison, Zhao et al. (2019) observed that the CMC-S-nZVI$_{One\text{-}step}$ particles were highly metamorphic and dominantly composed of lamellar structures, while the CMC-S-nZVI$_{Two\text{-}step}$ formed a typical spherical core–shell structure. For one-step sulfuration, Zhao et al. (2019) used at least 7 times more Na_2S than Xu et al. (2020e), which might explain the difference in particle morphology. However, more attention should be paid to the effect of stabilizers on the reactivity and aggregation of S-nZVI.

Alginate, a product extracted from algae, is composed of two various units (e.g., β–D-mannuronic acid and 1, 4-linked α-L-guluronic acid) in an asymmetrical arrangement. Moreover, an abundance of function groups, such as the carboxyl group and hydroxyl group, was observed in the units (Huang et al. 2016; Li et al. 2021a). It was proposed that the chemical conformation of alginate is adapted for modification of S-nZVI, making resultant composite with higher stability and reactivity. Li et al. (2021a) synthesized alginate-S-nZVI via one-step method in order to degrade TBBPA and found that the removal of alginate-S-nZVI for TBBPA could be achieved within 12 h. Moreover, the alginate-S-nZVI showed excellent longevity and reusability over S-nZVI, the rapid oxidization of S-nZVI was restrained by the alginate coating, and the reducing capability of S-nZVI

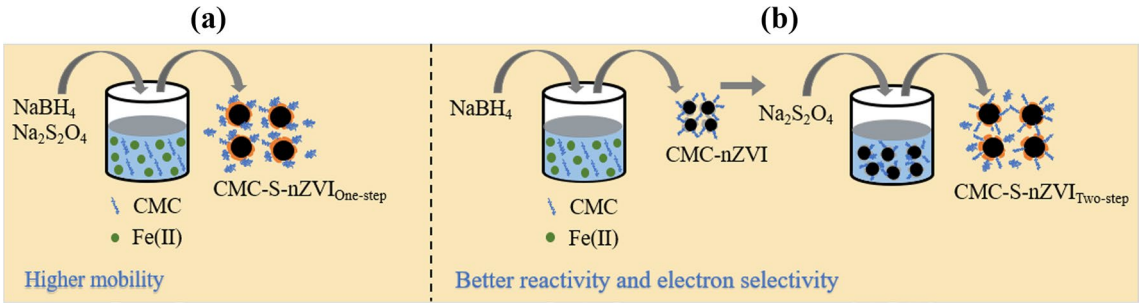

Fig. 4 Illustration of the synthesis procedures of CMC-S-nZVI$_{One\text{-}step}$ (**a**) and CMC-S-nZVI$_{Two\text{-}step}$ (**b**), respectively

was strengthened due to the generated Fe-alginate composites, both of which enhanced the removal performance of S-nZVI.

Environmental applications of S-nZVI

S-nZVI has been widely used in environmental remediation due to many merits, such as lo -cost, high reducing ability, strong reactivity, and selectivity. In this section, a range of S-nZVI-involved applications, including removal/immobilization of heavy metal, degradation of organic pollutants and removal of ARGs and ARB, are presented. Meanwhile, the reaction mechanisms of S-nZVI with various pollutants are described in Fig. 5.

Removal/immobilization of heavy metal

Heavy metals, such as chromium (Cr), arsenic (As), cadmium (Cd), lead (Pb), antimonite (Sb), and some radioactive elements are of great concern due to the non-degradability, toxicity, and bioaccumulation in water and soil. Recent studies on the removal or immobilization of heavy metal, metalloid, and radioactive elements by some representative S-nZVI-based materials are summarized in Table 2.

Cr

Cr is usually present in two different states: the trivalent form Cr^{3+} and the hexavalent form Cr^{6+}, which is prominently different in toxicity and mobility due to different oxidation states (Brumovský et al. 2021; Zhu et al. 2021). For instance, the Cr^{3+}, a trace nutrient element, is fundamental to human health, has low toxicity at elevated doses, and tends to form insoluble oxide and hydroxide precipitation, such as $Cr(OH)_3$ and $Cr_xF_{e(1-x)}(OH)_{3(s)}$ (Lv et al. 2019). On the contrary, the Cr^{6+} exerts major health concern due to its high oxidizing ability, resulting in mutagenic and carcinogenic effects (Du et al. 2016; Liu et al. 2022a). Moreover, Cr^{6+} always exists in chromate ($HCrO_4^-$, CrO_4^{2-}) and dichromate ($Cr_2O_7^{2-}$), which is extremely soluble and mobile in the natural environment (Brumovský et al. 2021; Guan et al. 2019). Generally, common techniques, such as reduction, adsorption and precipitation have been applied for Cr^{6+} removal (Guan et al. 2019; Lv et al. 2019). Recently, the efficacy of S-nZVI for Cr^{6+} removal has been demonstrated. The main removal process is that the Cr^{6+} is adsorbed onto the S-nZVI surface and then reduced to Cr^{3+}, and then forms of Cr^{3+} precipitates/co-precipitates (Eqs. 1, 2, 3, 4, 5, 6, 7, 8, and 9).

$$2HCrO_4^- + 14H^+ + 3Fe^0(s) \rightarrow 2Cr^{3+} + 8H_2O + 3Fe^{2+} \quad (1)$$

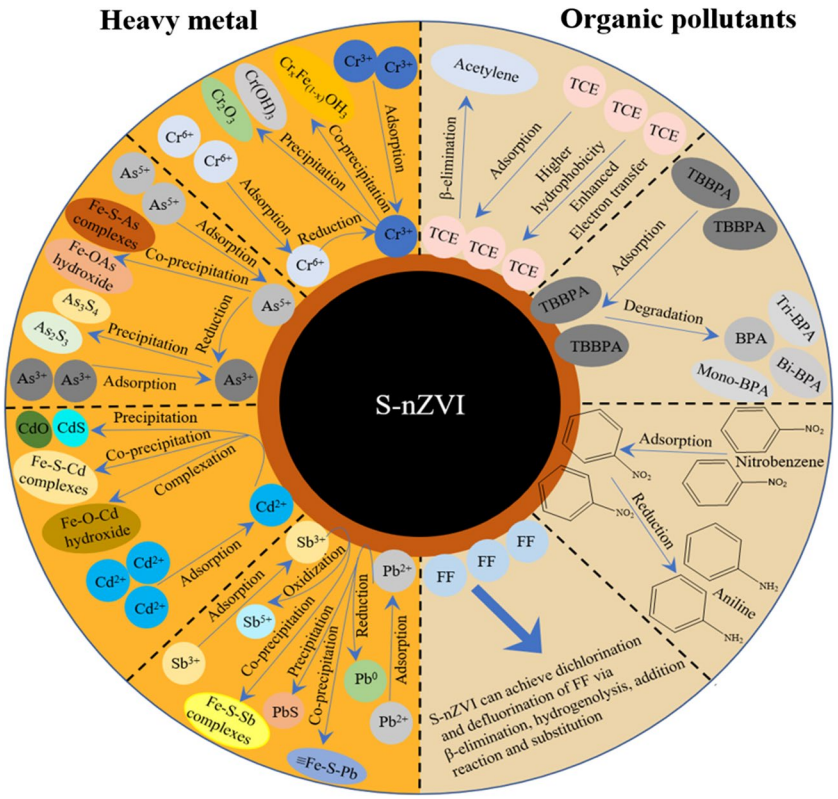

Fig. 5 Major mechanisms involved in the reactions of S-nZVI with heavy metals and organic pollutants

Table 2 Summary of representative S-nZVI-based materials for removal or immobilization of heavy metals

Materials	Contaminants	Contaminant concentration	Doses of materials	S/Fe	Reaction system	Time	Removal efficiency (%)	Kinetic model	References
S-nZVI	Cr (VI)	10–12 mg/L	4 g	N.A	Water	60 min	86	N.A	(Brumovský et al. 2021)
S-nZVI@BC	Cr (VI)	5–50 mg/L	N.A	0.25	Water	240 min	99.8	Pseudo-second-order	(Gao et al. 2018)
S-nZVI	Cr (VI)	10–40 mg/L	0.15 g	0.5	Water	120 min	N.A	Pseudo-second-order	(Lv et al. 2019)
S-nZVI	Cr (VI)	20 mg/L	0.1 g	0.11	Water	60 min	N.A	Pseudo-second-order	(Du et al. 2016)
S-nZVI@ABC	Cr (VI)	10–50 mg/L	N.A	0.25–1	Water	180 min	92.5	Pseudo-second-order	(Zhuang et al. 2021b)
S-nZVI	As (III)	5–50 mg/L	0.001 g	0.07–0.35	Water	120 min	N.A	N.A	(Wu et al. 2018)
S-nZVI	As (III)	10–50 mg/L	0.025 g	0.025–0.2	Water	120 min	99.7	Pseudo-second-order	(Singh et al. 2021)
S-nZVI@ZSM-5	As (V)	5 mg/L	0.01 g	0.05	Water	300 min	N.A	Pseudo-second-order	(Zhou et al. 2021a)
S-nZVI	As (V)	50 mg/kg	0.006 g	0.28	Soil	168 d	68	N.A	(Han et al. 2021)
S-nZVI	Cd (II)	10–60 mg/L	0.125 g	0.1–0.5	Water	15 min	100	Pseudo-second-order	(Lv et al. 2018)
S-nZVI	Cd (II)	2 mg/L	N.A	0.3	Water	60 min	100	Pseudo-first-order	(Li et al. 2021d)
S-nZVI	EDTA-Cd (II)	50–400 mg/L	0.03 g	0.75	Water	90 min	74.7	Pseudo-second-order	(Liang et al. 2021)
S-nZVI	Cd (II)	49.5 mg/kg	0.001g	0.75	Soil	N.A	97.6–100	N.A	(Guo et al. 2021)
S-nZVI@BC	Pb (II)	200 mg/L	0.05 g	0.2	Water	120 min	N.A	Avrami fractional-order	(Qu et al. 2021)
S-nZVI	Sb (III)	2–40 mg/L	0.01 g	0.02–0.1	Water	120 min	96.5	Pseudo-first-order and pseudo-second-order	(Liu et al. 2020b)

$$HCrO_4^- + 7H^+ + 3Fe^{2+} \rightarrow Cr^{3+} + 4H_2O + 3Fe^{3+} \quad (2)$$

$$8HCrO_4^- + 29H^+ + 3HS^- \rightarrow 8Cr^{3+} + 20H_2O + 3SO_4^{2-} \quad (3)$$

$$Cr_2O_7^{2-} + 3Fe^0 + 14H^+ \rightarrow 2Cr^{3+} + 7H_2O + 3Fe^{2+} \quad (4)$$

$$Cr_2O_7^{2-} + 6Fe^{2+} + 14H^+ \rightarrow 2Cr^{3+} + 7H_2O + 6Fe^{3+} \quad (5)$$

$$Cr_2O_7^{2-} + S^0 + 6H^+ \rightarrow 2Cr^{3+} + 3H_2O + SO_4^{2-} \quad (6)$$

$$4Cr_2O_7^{2-} + 3S^{2-} + 32H^+ \rightarrow 8Cr^{3+} + 16H_2O + 3SO_4^{2-} \quad (7)$$

$$2Cr^{3+} + 3S^{2-} \rightarrow Cr_2S_3 \quad (8)$$

$$2H_2O + xCr^{3+} + (1\text{-}x)Fe^{3+} \rightarrow Cr_xFe_{1-x}OOH(s) + 3H^+ \quad (9)$$

Brumovský et al. (2021) prepared S-nZVI for the removal of Cr^{6+} in the aquifer and found that the removal efficiency of S-nZVI for Cr^{6+} reached 86% and 100% within 60 min from Cr^{6+} spiked water and contaminated water, respectively. It was also observed that more than 95% of Cr was in the form of Cr^{3+}, corroborating the conversion of Cr^{6+} to Cr^{3+} after S-nZVI treatment. Besides, the S-nZVI amendment would decrease the redox potential of groundwater, which was also conducive to the reduction of Cr^{6+}. Similarly, Gao et al. (2018) applied S-nZVI@BC to remove Cr^{6+} from water. It was demonstrated that a S-nZVI@BC injection followed by a rapid decrease of Cr^{6+} concentration within 60 min and the removal efficiency was closed to 100% within 4 h. In this work, the scavenging of Cr^{6+} was

believed to begin with adsorption, which was facilitated by the oxygen functional groups (e.g., C = O, Si–O, and -OH) of BC and adsorption sites provided by S-nZVI. Cr^{6+} was then reduced into Cr^{3+} by S-nZVI. Meanwhile, $Cr(OH)_3$ and Cr_2O_3 precipitates were formed via precipitation between Cr^{3+} and S-nZVI. A novel kind of FeS@Fe^0 composite was fabricated by Du et al. (2016) for the reductive sequestration of chromate. It was found that the maximum adsorption capacity of FeS@Fe^0 towards Cr^{6+} was 66.7 mg/g. Moreover, it was also ascertained that the adsorption process of Cr^{6+} by S-nZVI was consistent with pseudo-second-order kinetic model. In the process of reducing Cr^{6+} to Cr^{3+}, the Fe^{2+} species generated from the Fe^0 corrosion and FeS disintegration played a dominant role over direct electron transfer from Fe^0 and oxidization of sulfur species (e.g., FeS, FeS_2, and S^0). At the end of the removal process, the Cr^{3+} then was immobilized as Fe–Cr hydroxide precipitates (Du et al. 2016; Gao et al. 2018; Gong et al. 2017). Moreover, it was also reported that the reduced Cr^{3+} may occurred as insoluble Cr_2O_3 and $FeCr_2S_4$ (Gao et al. 2018; Gong et al. 2017). Notably, the FeS_x shell plays a crucial role in the removal of Cr^{6+} by S-nZVI: (1) facilitate the electron transfer from Fe^0, (2) provide adsorption sites, and (3) produce reductive species (e.g., Fe^{2+} and S^{2-}).

As

As, a confirmed carcinogen, is commonly found in groundwater in the form of arsenate (As^{5+}) and arsenite (As^{3+}) (Han et al. 2021; Zhao et al. 2021b). Compared with As^{5+}, the As^{3+} is more toxic, mobile, and easily dissolved into water (Wu et al. 2018). To date, S-nZVI has been proved to efficiently immobilize the As in the natural environment. The removal process of As by S-nZVI involved a series of mechanisms, including adsorption, reduction, co-precipitation, and oxidization (Han et al. 2021; Singh et al. 2021; Wu et al. 2018). Singh et al. (2021) found that the removal efficiency of S-nZVI towards As was superior to that of nZVI and the introduction of sulfide changed the removal mechanism of As by nZVI. Adsorption of As^{3+} and As^{5+} and reduction to As^0 were identified as the main removal mechanisms of nZVI towards As. However, the removal mechanisms of S-nZVI towards As were adsorption, precipitation of As_2S_3-like phase and co-precipitation of Fe-As hydroxide. Wu et al. (2018) demonstrated that the maximum removal capacity of As^{3+} by S-nZVI was 240 mg/g. It was observed from the characterization results that adsorption by forming inner-sphere complexes, precipitation of FeAsS-like phase and co-precipitation of Fe-As hydroxide contributed to the As^{3+} removal by S-nZVI, among which co-precipitation played the dominating role. Zhou et al. (2021a) proved the high efficacy of S-nZVI@ZSM-5 in the removal of As^{5+} from $CuSO_4$ effluent. The following processes were mainly involved in the removal of As^{5+} by S-nZVI@ZSM-5: (1) the electrostatic interaction between As^{5+} and S-nZVI@ZSM-5 resulted in the As^{5+} being adsorbed onto the S-nZVI@ZSM-5 surface, (2) the redox reaction between As^{5+} and Fe^{2+} contributed to the generation of As^{3+} (Eq. (10)), (3) the interaction between As^{5+} and FeOOH leaded to the formation of Fe–O-As coprecipitates (e.g., $Fe_8As_{10}O_{23}$ and Fe_3AsO_7) (Eq. 11). Han et al. (2021) reported that S-nZVI has a roughly twofold greater immobilization capacity for As^{5+} than nZVI in soil. The immobilization of S-nZVI to As^{5+} was improved by the presence of sulfhydryl (-SH) in S-nZVI, and the fixed products were mainly FeAsS and As_4S_4.

$$2Fe^{2+} + As^{5+} \rightarrow 2Fe^{3+} + As^{3+} \quad (10)$$

$$As(+3,\ +5) + \equiv Fe(+2,\ +3) \rightarrow \equiv Fe(+2,\ +3)\ \text{containing}\ As(+3,\ +5)\ \text{phases} \quad (11)$$

Cd

Cd is a carcinogenic heavy metal and has been listed as a priority pollutant due to its bioaccumulation, toxicity and recalcitrance (Lv et al. 2018). S-nZVI has been proved to be effective at immobilizing Cd, consequently decreasing the mobility, bioavailability and toxicity of Cd, by means of chemical adsorption, ion exchange, surface complexation, and co-precipitation. The surface complexation between Cd^{2+} and iron (oxyhydr)oxides or $\equiv FeSH^+$ (Eqs. 12, 13, and 18), chemical precipitation between Cd^{2+} and dissolved S^{2-} (Eqs. 14, 15, and 16), the ion exchange between Cd^{2+} and FeS (Eq. 17), and the co-precipitation between Cd^{2+} and $FeSH^+$ (Eq. 19) are associated reactions in the Cd^{2+} removal by S-nZVI (Lv et al. 2018; Su et al. 2015).

$$Cd^{2+} + \equiv FeO^- \rightarrow \equiv FeOCd^+ \quad (12)$$

$$Cd^{2+} + \equiv FeOH + H_2O \rightarrow 2H^+ + \equiv FeOCdOH \quad (13)$$

$$FeS_{(s)} + H^+ \rightarrow Fe^{2+} + HS^- \quad (14)$$

$$Cd^{2+} + HS^- \rightarrow CdS_{(s)} + Fe^{2+} \quad (15)$$

$$Cd^{2+} + FeS_{(s)} \rightarrow CdS_{(s)} + Fe^{2+} \quad (16)$$

$$xCd^{2+} + \equiv FeS \rightarrow \equiv Fe_{(1-x)}Cd_xS + xFe^{2+} \quad (17)$$

$$Cd^{2+} + \equiv FeSH^+ \rightarrow \equiv FeS - Cd^{2+} + H^+ \quad (18)$$

$$xCd^{2+} + FeSH^{+} \rightarrow Fe_{(1-x)}Cd_xS + xFe^{2+} + H^{+} \quad (19)$$

Lv et al. (2018) found that S-nZVI could achieve complete removal of Cd in 15 min and the removal process exhibited good conformity with the pseudo-second-order kinetic model. Moreover, a maximum removal capacity of roughly 150 mg/g was obtained at the S/Fe molar ratio of 0.3. The iron hydroxides on the surface of S-nZVI could be used to immobilize Cd^{2+} via surface complexation forming ≡FeOCdOH. Meanwhile, the FeS also contributed to the removal of Cd^{2+} with the generation of ≡FeS-Cd^{2+} via surface complexation and $CdS_{(s)}$ via precipitation (Fig. 6a). Meanwhile, Su et al. (2015) found that the immobilization mechanisms of S-nZVI for Cd were in discrepancy under different S/Fe molar ratio. It was revealed by the XPS characterization results that adsorption and surface complexation were responsible for the Cd immobilization under low S/Fe molar ratio, whereas the Cd was immobilized via ion exchange forming Cd-Fe sulfide phase under high S/Fe molar ratio. The immobilization efficacy and mechanism of Cd contaminated soil by S-nZVI were also proposed by Guo et al. (2021). It was observed that the exchangeable fraction of Cd was decreased by 97% after 30 days of treatment, which evidently decreased the mobility of Cd. The immobilization of Cd by S-nZVI was successfully conducted, and CdO and CdS were the primary immobilization products. Besides, the ultimate corrosion products of S-nZVI (e.g., α-FeOOH, γ-FeOOH, and γ-Fe_2O_3) were also conducive to the adsorption of Cd.

EDTA, as a powerful chelate, is easy to form stable complex with Cd, which is more difficult to remove over common metal ions (Li et al. 2021d). Traditional methods, such as chemical precipitation, physical adsorption, and redox reaction, cannot effectively achieve complete removal of EDTA-Cd (Li et al. 2021d; Liang et al. 2021). The effectiveness of S-nZVI for removal of EDTA-Cd has been proved (Liang et al. 2020). For example, Liang et al. (2021) demonstrated that S-nZVI had a removal capacity of 746.6 mg/g of EDTA-Cd within 90 min. The Cd ions were released from the EDTA-Cd complex via the replacement of Fe^{3+}; then, the free Cd ions were immobilized on S-nZVI via the second replacement of FeS, leading to the formation of CdS. Li et al. (2021d) proposed that the complete removal of low-concentration of EDTA-Cd by S-nZVI could be achieved even in high-salinity wastewater. Similarly, the Cd^{2+} of EDTA-Cd was firstly replaced by the Fe^{3+} derived from the corrosion of S-nZVI, and then the free Cd^{2+} was immobilized on S-nZVI producing CdS and Fe–O-Cd (Fig. 6b).

Pb and Sb

Pb, a common heavy metal, is highly toxic and easily accumulated via the food chain, which poses adverse effects on the brain, kidney, and nerve system of human (Qin et al. 2022). Sb is known for its high toxicity and carcinogenicity, which can lead to a number of diseases, including hemolysis and pulmonary edema (Wang et al. 2018). Qu et al. (2021) proposed that S-nZVI@HPAC was able to bind 295.3 mg/g of Pb^{2+} within 2 h. The Pb^{2+} was absorbed onto the negatively charged surface of S-nZVI@HPAC via electrostatic attraction, and the carbon-containing functional groups (e.g., C-O, C–C, and C-H) of HPAC also facilitated the adsorption process. The surface complexation occurred when Pb^{2+} reacted with iron (hydroxyl)oxides and FeS, respectively, and some oxygenous groups (e.g., C = O, C–O–C, and -OH) were also involved in the formation of Pb^{2+} complexes. Besides, the Pb^{2+} could also be removed via chemical precipitation between FeS and Pb^{2+} forming PbS precipitates. More importantly, a fraction of Pb^{2+} could be reduced into Pb^0 by Fe^0. In another study, rhamnolipid stabilized S-nZVI (RL@S-nZVI) had a 22% greater immobilization

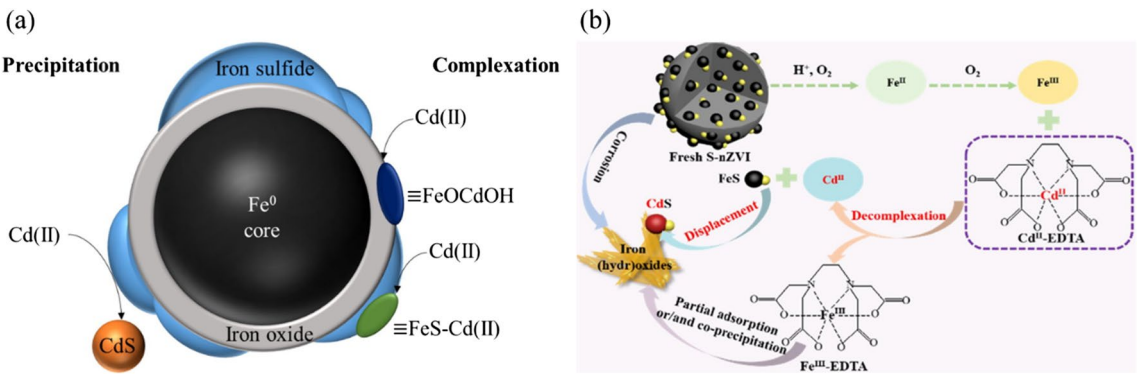

Fig. 6 The mechanism for Cd immobilization by S-nZVI (**a**). Reprinted with permission from Ref. (Lv et al. 2018). Copyright 2018, Elsevier. And for EDTA-Cd immobilization by S-nZVI (**b**). Reprinted with permission from Ref. (Liang et al. 2021). Copyright 2021, Elsevier

efficiency for Pb^{2+} than pure nZVI, and RL@S-nZVI was able to stabilize water-soluble Pb with a stabilization efficiency of up to 63% even in the coexistence of Cd and As. The Pb^{2+} was removed via ion exchange with FeS forming PbS/PbO precipitates, reduction into Pb^0 by Fe^0 and surface complexation with FeS and iron (hydroxyl) oxides forming Pb^{2+} complexes (Song et al. 2023). Liu et al. (2020b) demonstrated that S-nZVI could remove Sb^{3+} with a removal efficiency of up to 96.5% and 64.3%, respectively, under aerobic and anaerobic situation within 2 h. The Sb^{3+} could be effectively removed via oxidization into Sb^{5+} by ·OH derived from S-nZVI, adsorption onto the S-nZVI or its corrosion products, and precipitation in the form of Fe-S-Sb. Graphene oxide–supported S-nZVI (S-nZVI@GO) was synthesized by Chi et al. (2022) to further enhance the Sb^{3+} removal by S-nZVI. In their study, it was found that S-nZVI@GO had a maximum adsorption capacity for Sb^{3+} of 311.75 mg/g within 2 h and the removal efficiency of Sb^{3+} of up to 96.7%. During the removal process, Sb^{3+} was firstly oxidized into Sb^{5+} by active oxygen species, which was derived from S-nZVI@GO via single-electron transfer. Then, the remained Sb^{3+} and generated Sb^{5+} were further removed by adsorption and co-precipitation.

Radioactive metals

Moreover, it has also been proposed that S-nZVI had outstanding removal performance towards radioactive metals. Pang et al. (2019) discovered that S-nZVI loading with biochar, derived from *Dictyophora* indusiate, had a removal capacity for U^{6+} of up to 427.9 mg/g within 3 h, and the adsorptive and reductive effect were responsible for the excellent removal effects. Two works by Fan et al. (2013) and Fan et al. (2014) proposed that S-nZVI could effectively improve the sequestration efficiency of TcO_4^- forming TcS_x rather than TcO_2, which was more resistant to oxidization. Besides, the long-term antioxidant ability of TcS_x was also confirmed.

In light of the discussions above, it may be claimed that S-nZVI-based composites possess high removal efficiency towards various metallic ions. The involved removal mechanisms mainly include reduction, adsorption, precipitation, or the synergistic effect of multiple mechanisms. Meanwhile, the removal effect of S-nZVI on the coexistence of multiple heavy metal pollution in environmental media still needs to be further explored.

Removal of organic pollutants

To date, it was widely acknowledged that the efficacy of S-nZVI applied for the elimination of a variety of organic pollutants, mainly including TCE (Bhattacharjee and Ghoshal 2018b; He et al. 2018), TBBPA (Gao et al. 2023; Li et al. 2016), NB (Gao et al. 2022a; Zhang et al. 2020b), and antibiotics (Dong et al. 2019b; Zhang et al. 2023). The latest studies on the application of S-nZVI-based materials for degradation of organic pollutants are summarized in Table 3.

TCE

As one of the most prevalent chlorinated organic compounds in groundwater and soils, TCE was featured by toxicity, carcinogenicity, and recalcitrance and has led to significant environmental problems for decades (Baldermann et al. 2021; Dong et al. 2017). To date, a few studies have revealed that S-nZVI has excellent TCE removal performance. For example, Kim et al. (2011) prepared Fe/FeS nanocomposites by adding $Na_2S_2O_4$ into the synthetic solution of nZVI, and the TCE removal rate was increased by 20 times. Mangayayam et al. (2019) utilized S-nZVI to degrade TCE and also found that S-nZVI could remove more than 99% of TCE, while that by nZVI was only about 40%. Moreover, the aging experiments indicated that the retention rate of S-nZVI for TCE removal was higher than 50% even after 30 days of reaction. Bin et al. (2020) applied S-nZVI/GA to remove TCE in the water. The results showed that S-nZVI/GA could completely remove TCE within 50 min, with acetylene being the primary dechlorination product of TCE. The reasons why S-nZVI was more reactive to TCE compared to nZVI have been explored by some researchers. According to Mangayayam et al. (2019), the FeS shell of S-nZVI was found to be more conductive compared to the iron oxides shell of nZVI, resulting in faster electron shuttle from Fe^0 to pollutants. The increase of FeS shell volume further promoted the electron transfer leading to faster TCE reduction, and atomic S on the S-nZVI surface could induce β-elimination for producing acetylene. Gu et al. (2017) proposed that the FeS not only facilitated the electron shuttle but also enhanced the electron selectivity. The electrons were preferentially transferred to TCE over H^+ and its transfer efficiency increased from 8 to 87%. Different from previous studies, Han and Yan (2016) observed that the degradation efficiency of S-nZVI for TCE was 60-fold higher than nZVI and the degradation products were totally dechlorinated hydrocarbons. It was demonstrated that sulfur was not a direct promoter of the TCE dechlorination reaction, but rather a modifier of the surface chemistry of iron to facilitate the production of key reactive species in the TCE reduction process. When sulfur was deposited on the surface of iron, it induced the dissolution of natural oxides, making the surface more conducive to the adsorption of atomic hydrogen. At the same time, inhibiting the recombination of hydrogen promoted

Table 3 Summary of representative S-nZVI-based materials for degradation of organic pollutants

Materials	Contaminants	Contaminants concentration	Doses of materials	S/Fe	Reaction system	Time (min)	Removal efficiency (%)	Kinetic model	References
S-nZVI	TCE	25 mg/L	0.15 g	0.00125–0.75	Water	800	N.A	Pseudo-first-order	(Han and Yan 2016)
S-nZVI	TCE	40 mg/L	0.15 g	0.02	Water	8	66	N.A	(Wang et al. 2020a)
S-nZVI	TCE	0.11mM	0.022–0.074 g	0.002–0.247	Water	390	58	Pseudo-first-order	(Rajajayavel and Ghoshal 2015)
S-nZVI@GA	TCE	20 mg/L	0.05 g	0.098	Water	50	100	Pseudo-first-order	(Bin et al. 2020)
S-nZVI	TCE	30 mg/L	0.1 g	0.01–0.1	Water	540	100	N.A	(Dong et al. 2018)
S-nZVI	TBBPA	20 mg/L	0.23 g	0.51	Water	1440	90	Pseudo-first-order	(Li et al. 2016)
S-nZVI	TBBPA	20 mg/L	0.23 g	0.015–0.25	Water	120	91.4	Pseudo-first-order	(Wang et al. 2021)
S-nZVI@BC	DCF	10 mg/L	0.04 g	N.A	Water	240	80.1	N.A	(Xu et al. 2021)
S-nZVI	NB	100 mg/L	0.1 g	0.3	Water	10	60.2	Pseudo-first-order	(Zhang et al. 2018)
S-nZVI	FF	0.28 mM	0.5 g	0–0.28	Water	120	46–90	Pseudo-first-order	(Cao et al. 2017)
S-nZVI	FF	0.28 mM	0.25 g	0.07–0.28	Water	120	100	Pseudo-first-order	(Cao et al. 2020)
S-nZVI@PS	SMX	10 mg/L	0.5–4.5 mM	0.2	Water	60	97.5	Pseudo-first-order	(Yu et al. 2022b)
S-nZVI@BC-PS	CIP	30 mg/L	0.1 g	0–0.5	Water	100	99.01	Pseudo-second-order	(Gao et al. 2020)
S-nZVI@PS	CAP	20 mg/L	0.005–0.03 g	0.025–0.1	Water	30	98.8	Pseudo-first-order	(Wu et al. 2022a)
S-nZVI@PMS	TC	20 mg/L	25–175 mg/L	0.2	Water	20	93.8	Pseudo-first-order	(Yu et al. 2022a)

the accumulation of atomic hydrogen on the surface of iron and reacted with TCE (Fig. 7a). In addition, Garcia et al. (2020a) proposed that the injection of CMC-S-nZVI to a site contaminated with chlorinated volatile organic compounds (cVOCs) brought about short-term abiotic dechlorination leading to a rapid decrease of cVOCs concentration, followed by the long-term biotic dechlorination. It was also found that CMC-S-nZVI migration to the monitoring well, either up or down gradients, leaded to a considerable reduction in cVOCs concentration in the water phase (Fig. 7b). In the above process, there might be a continuous transformation mechanism of hydrogenation and reducing β-elimination. Therefore, the dichlorination process of TCE by S-nZVI may involve abiotic and biotic transformation and further research on biotic transformation mechanism is crucial for TCE removal.

TBBPA

TBBPA is a widely used brominated flame retardant (BFR) that causes significant damage to human health and ecosystem due to random discharge and improper handling (Okeke et al. 2022). Many treatment methods have been proposed for removal or degradation of TBBPA, such as adsorption, catalytic degradation, and biodegradation (Macêdo et al. 2022; Ye et al. 2022). Although the methods above could eliminate TBBPA from different environment matrices, it still faced some limitations in the application scenario. For example, adsorption could not easily remove the generated byproducts, the degradation rate of TBBPA by catalytic reaction was always slow and the biodegradation demanded a relatively long degradation cycle (Dong et al. 2022; Li et al. 2020; Yuan et al. 2021). Recently, some studies have demonstrated that S-nZVI exhibited a high removal efficiency towards BFR. For instance, Li et al. (2016) observed that S-nZVI was able to degrade TBBPA with a degradation efficiency of 90% within 24 h and the transformation rate of S-nZVI for initial TBBPA was 55.5% even after 11 weeks of aging. It was also proposed that the excellent transformation capacity of S-nZVI toward TBBPA was ascribed to the formation of FeS, resulting in elevated electron transfer and oxidative resistance. TBBPA might undergo a continuous pathway of debromination, forming products that are low in bromine or even free of bromine. In each stage, only

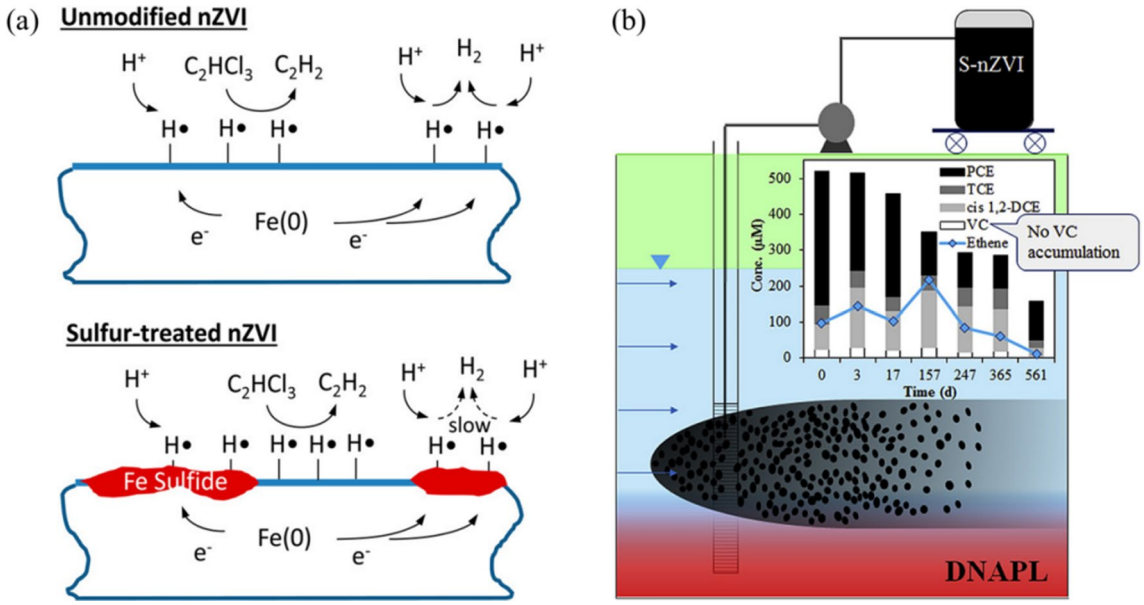

Fig. 7 **a** Reaction mechanisms of TCE by nZVI and S-nZVI. Reprinted with permission from Ref. (Han and Yan 2016). Copyright 2016, American Chemical Society. **b** CMC-S-nZVI was applied at a site contaminated by cVOCs. Reprinted with permission from Ref. (Garcia et al. 2020a). Copyright 2020, Elsevier

one bromine atom might be replaced by a hydrogen atom (Fig. 8a). Wang et al. (2021) prepared S-nZVI using S^0 as sulfur source for the removal of TBBPA and found that S-nZVI could transform more than 90% of TBBPA within 2 h with optimal S/Fe molar ratio at 0.025. It was because of the generation of iron sulfide layer on S-nZVI surface that significantly increased its hydrophobicity and decreased the electron resistance, leading to superior transformation rate of TBBPA. Some studies have been conducted to enhance the degradation performance of TBBPA through modified S-nZVI. Li et al. (2021b) successfully synthesized a S-nZVI-based composite loading with dendritic mesoporous silica nanospheres (S-nZVI/DMSN). It can be drawn from the characterization results and degradation experiments that both the dispersion of S-nZVI particles and the pollutants accessibility to S-nZVI particles were largely enhanced with the introduction of dendritic pores (Fig. 8b–d). The removal efficiency of S-nZVI/DMSN for TBBPA was up to 91.4%, which was higher than that of S-nZVI (66.3%) when the mass ratio of Si/Fe was 1.0 and the molar ratio of S/Fe was 0.1 (Fig. 8e). The elimination of TBBPA by S-nZVI/DMSN could be divided into three stages. Firstly, the physical adsorption caused the adhesion of TBBPA on S-nZVI/DMSN. Secondly, TBBPA was chemically reduced by the S-nZVI distributed in DMSN. In addition, the Fe^{2+} and H_2, as reaction products, could also provide reducing capacity. Thirdly, the diffusion of the TBBPA debromination products into the solution occurred (Fig. 8f). The transport of target molecules to the active region of S-nZVI nanoparticles was considerably improved and accelerated by the distinctive dendritic pore structure of DMSN.

NB

NB is extensively used in the manufacture of explosives, pesticides, and organic solvents (Gao et al. 2022a). Consequently, it was frequently detected in the environment as a typical nitroaromatic compound of great concern. S-nZVI as a reducing agent was oxidized transferring electrons to the target pollutants, thereby transforming toxic substances into non-toxic or less toxic species (Zhang et al. 2019b, 2020b). To date, several studies on the application of S-nZVI for NB removal have been conducted to reveal the removal efficiency and corresponding mechanisms. Zhang et al. (2018) observed that S-nZVI@BC was able to remove NB completely within 30 min and had a removal capacity of up to 588.23 mg/g. Under the synergistic action of S-nZVI and BC, the NB was removed mainly through the chemisorption and electron shuttle by S-nZVI@BC and the chemical reduction by S-nZVI. Similarly, Gao et al. (2022a) reported that the degradation rate of NB by S-nZVI@BC was 98% and the formation rate of p-aniline (AN) was 90% within 24 h under the mass ratio of S-nZVI/BC of 3: 1 and the dosage of 10 mg/g (Fig. 9a–d). As shown in Fig. 9e, the nitro groups were desorbed from the soil via carbon phase solubilization by BC and reduced into amino groups by S-nZVI via direct electron shuttle of FeS_x. Note that the NB removal efficiency is not equal to NB reduction

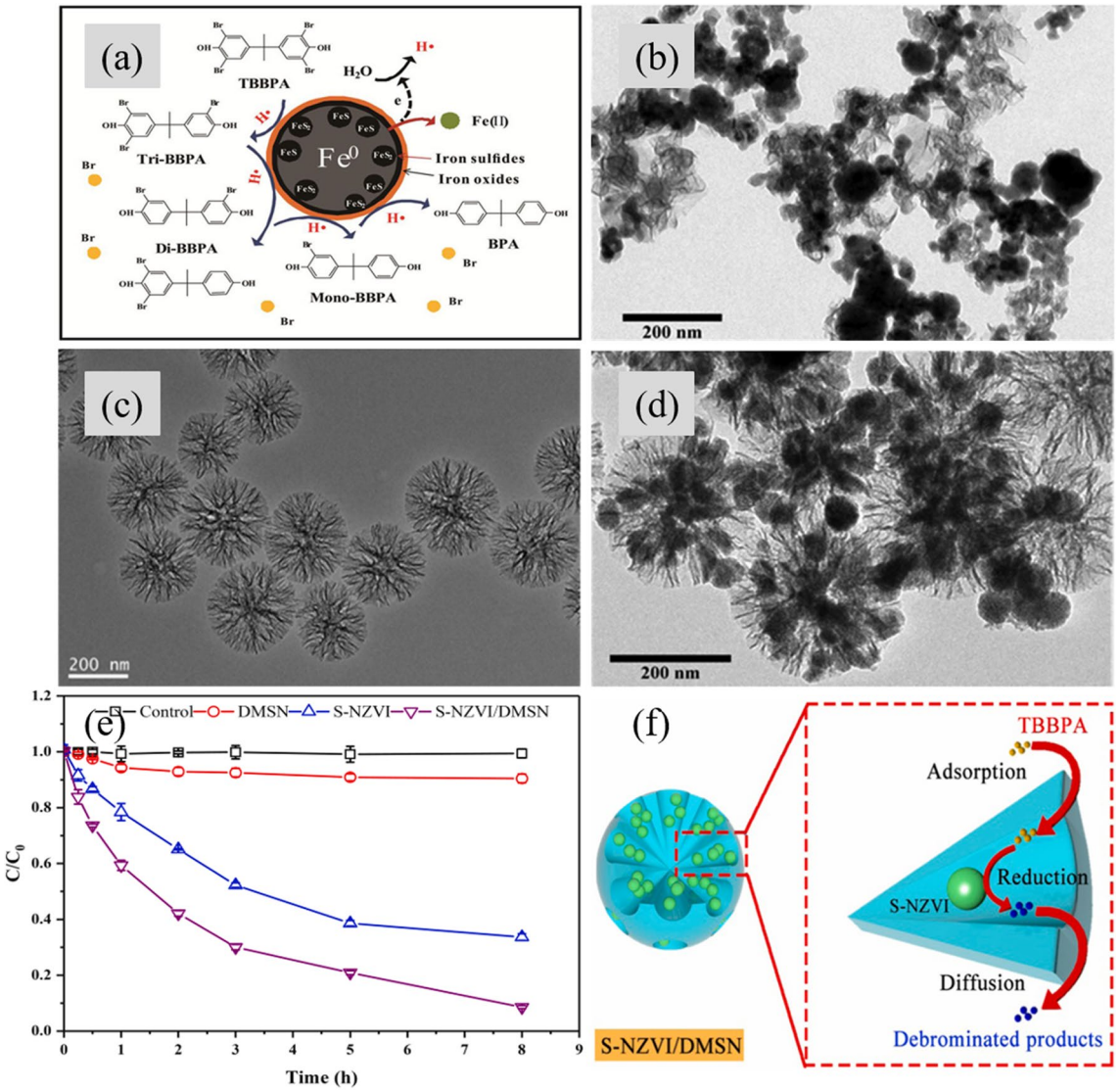

Fig. 8 **a** The debromination pathway of TBBPA with the treatment by S-nZVI. Reprinted with permission from Ref. (Li et al. 2016). Copyright 2016, Elsevier. TEM images of **b** S-NZVI, **c** DMSN, and **d** S-NZVI/DMSN. **e** Degradation efficiency of TBBPA as a function of time by different materials. **f** Removal mechanisms of TBBPA by S-NZVI. Reprinted with permission from Ref. (Li et al. 2021b). Copyright 2021, Elsevier

efficiency, but is generally represented by the aniline (AN) formation efficiency. Some investigations reported that S-nZVI coupled anaerobic system was economic, effective, and beneficial to further improve the applicability of S-nZVI toward NB-contaminated sites. Zhang et al. (2020b) coupled S-nZVI with anaerobic sludge for the removal of NB from wastewater. It was observed that complete NB removal was achieved within 32 h at 0.3 of S/Fe molar ratio, in which AN formation efficiency was evidently improved to about 76.4% compared to 8.3% of the anaerobic control system. Supplement of S-nZVI largely promoted the NB reduction and the positive role of microbial community. Furthermore, Zhang et al. (2019b) added S-nZVI@BC to the up-flow anaerobic sludge blanket (UASB) for the reduction of NB. It was found that the removal efficiency of NB and the formation efficiency of AN by S-nZVI@BC coupled UASB reached up to nearly 100% and 20–40%, respectively. The application of S-nZVI@BC significantly enhanced the stability of anaerobic system and enriched the microbes related to NB reduction.

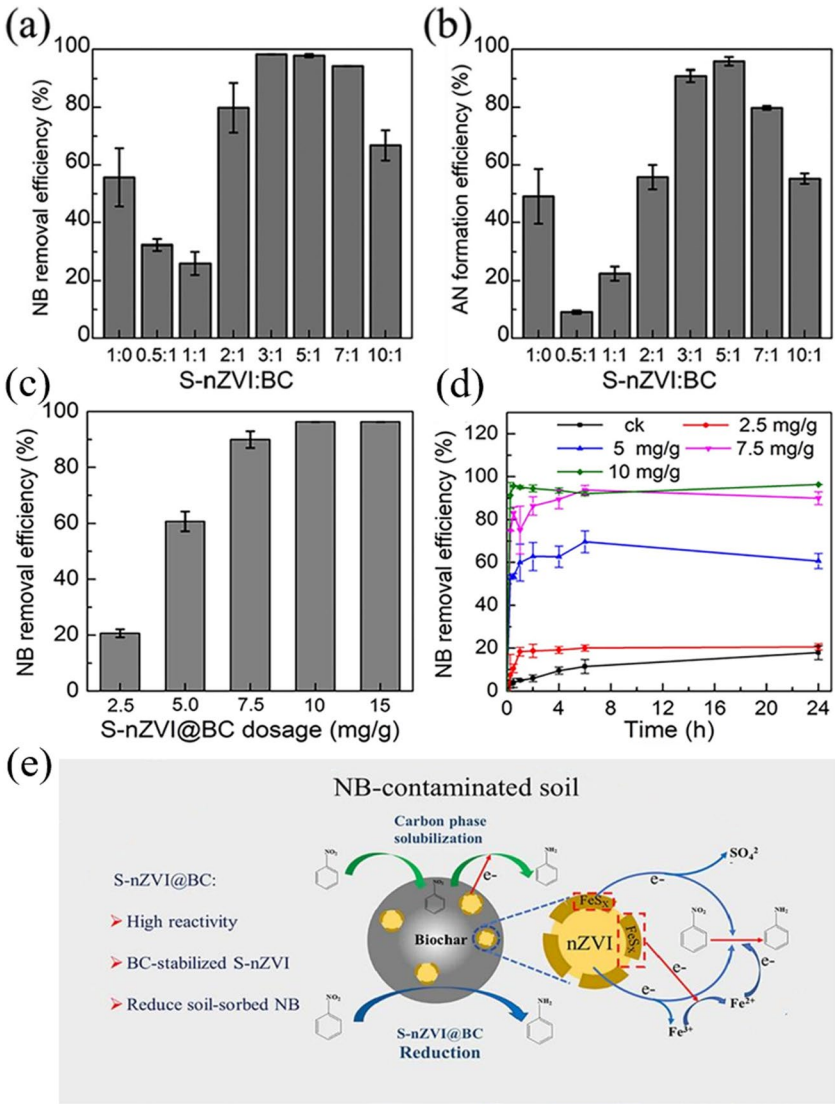

Fig. 9 **a** Effect of S-nZVI/BC mass ratio on the NB removal efficiency. **b** The formation of AN. **c** Effect of S-nZVI/BC dosage on the NB removal efficiency. **d** NB removal efficiency at different times. **e** Reaction mechanisms of NB by S-nZVI/BC in contaminated soil. Reprinted with permission from Ref. (Gao et al. 2022a). Copyright 2022, Elsevier

Antibiotics

Antibiotics are often used to treat infectious diseases and are also common in agriculture and livestock industry (Gao et al. 2020). The common removal methods of antibiotics included physical–chemical (e.g., UV radiation, ozonation, and chlorination), chemical (e.g., PS, UV/H_2O_2, and Fenton reactions) and biological strategies (Wu et al. 2022a; Yu et al. 2022b; Zhang et al. 2020d). Indeed, S-nZVI has been proved as an effective material for the removal of various antibiotics, such as florfenicol (FF) (Cao et al. 2021), sulfamethoxazole (SMX) (Yu et al. 2022b), chloramphenicol (CAP) (Wu et al. 2022a), ciprofloxacin (CIP) (Gao et al. 2020), and tetracycline (TC) (Yu et al. 2022a). Recent studies of some representative S-nZVI-based materials for the degradation of antibiotics are summarized in Table 3. Among them, FF is discussed in this section.

FF is an antibiotic which is often detected in the natural environment for its wide use in the aquaculture and prevention of several human diseases (Cao et al. 2017). The effective degradation pathway of FF involved either dechlorination or defluorination, both of which can destruct the molecule structure of FF. Moreover, defluorination is more difficult than dechlorination as a result of C-F is more stable than C–Cl. Up to date, the feasibility and effectiveness of S-nZVI for degradation of FF have been proved by previous research. For example, Cao et al. (2017) proposed that the removal efficiency of S-nZVI towards FF was more than 46% after 2 h, while nearly no FF removal was observed in the nZVI treatment group. The dechlorination of S-nZVI for FF was a continual process, in which chlorine atom was removed one by one. Meanwhile, it was also demonstrated that dissolved oxygen promoted the partial defluorination of S-nZVI for FF. Successive dichlorination (100% in 3 days) and defluorination (45% in 15 days) of S-nZVI for FF was

found by Cao et al. (2020) under ambient conditions. S-nZVI particles containing higher contents of S^{2-} and S_2^{2-} substances displayed a faster dechlorination and defluorination rate for FF. It was suggested that the dechlorination and defluorination of S-nZVI for FF was achieved via β-elimination, substitution, hydrogenolysis, and addition reactions. Importantly, the distinctive core–shell structure, sulfur content and Fe^0 content of S-nZVI particles synthesized by different sulfurization methods caused variations in the dechlorination and defluorination rates of S-nZVI for FF, whereas the sulfur content and sulfurization method had no effect on the degradation pathway of S-nZVI for FF. Therefore, S-nZVI is a promising technology for removing fluoride at room temperature and pressure.

According to the discussion above, S-nZVI has proved to be an excellent remediation material for the degradation of various organic pollutants. However, the current application of S-nZVI is limited to a few specific types of organic pollutants and more applications should be explored. Also, further efforts are required to clarify the exact role of S in these reactions, especially in defluorination reactions.

Removal of ARGs and ARB

The overuse and continuous release of antibiotics promote the formation and spread of ARGs and ARB, which has been a public health of concern for increasing the resistance of pathogenic bacteria and reducing the efficacy of antibiotics against human and animal pathogens (Gao et al. 2020; Wang et al. 2020b; Zhang et al. 2020d). Studies have shown that ARGs and ARB are widely distributed in various environmental media, such as rivers, lakes, soil, vegetables, and even air, and have been considered as a new type of environmental pollutants (Zhuang et al. 2021a). In addition, the movement of mobile genetic elements (MGEs, e.g., transposons, integrons, and plasmids) containing ARGs can achieve horizontal gene transfer (HGT) of ARGs between or within species (Liu et al. 2022c; Wang et al. 2020b). Currently, various treatment methods such as activated sludge, chlorination disinfection, and advanced oxidation process, have been widely utilized for removal of ARB and ARGs (Foroughi et al. 2022; Li et al. 2022b; Wang et al. 2023). Although these technologies can inhibit the enrichment of ARGs or ARB to some extent through mechanisms such as adsorption and degradation, their effectiveness is not ideal. In recent years, some studies have explored the impact of S-nZVI on ARGs and ARBs and shown that S-nZVI was effective for reducing the proliferation of ARB and ARGs through adsorption, oxidization, and reduction. Wang et al. (2020b) investigated the inactivation of S-nZVI against sulfonamide-resistant bacteria (ARB HLS.6) and the removal of intracellular ARGs (*sul1*) and Class I integrase genes (*intI1*). Results analysis showed that untreated ARB cells were morphologically and structurally intact (Fig. 10a, b). After 15-min reaction, the cell structure of ARB was seriously disrupted in S-nZVI system (Fig. 10c, d). Figure 10e, f exhibited more severe cell damage, complete lysis of ARBs, and leakage of intracellular components. 1.12 g/L S-nZVI (S/Fe = 0.1) could completely inactivate ARBs (2×10^7 CFU/mL) within 15 min, and the removal rates of intracellular *sul1* and *intI1* reached 4.39 log and 4.67 log after 60 min, respectively. These results indicated that the genetic function and activity of ARB might be permanently disrupted after S-nZVI treatment, which inhibited the regeneration of ARGs. It can be seen from the quenching experiments that ROSs produced by materials played a crucial part in inactivating ARBs and eliminating genes. Additionally, the removal of ARB and genes from water could be achieved by S-nZVI and its oxidation products by means of adsorption. Zhang et al. (2020d) proposed that S-nZVI was an effective material for the elimination of 16S rRNA, ARGs, and MGEs in secondary effluents from wastewater treatment plants. Quantitative PCR (qPCR) and high-throughput fluorescence qPCR results showed that S-nZVI treatment could remove 16S rRNA from secondary effluent by more than 3 log units, and 7 out of 10 ARGs could be removed. Specifically, the 16S rRNA was firstly adsorbed onto the surface of S-nZVI, then accepted the electron transferred from the Fe^0 resulting in the decrease of 16S rRNA and ARGs, and the loss of regenerative ability, especially the typical MGE (*intI1*). Moreover, the efficacy of S-nZVI on inactivating donor and recipient bacteria has been demonstrated by destroying the membrane, producing excessive ROS and reducing the expression of ARGs, thereby reducing the horizon gene transfer in the process (Liu et al. 2022c).

The effectiveness of S-nZVI for degradation ARB and ARGs has been confirmed and the relation between influencing factors (e.g., S/Fe molar ratios, S-nZVI dosages, initial pH, or initial concentration of pollutants) and degradation performance was imperative to be clarified.

Factors influencing the effectiveness and properties of S-nZVI

Though S-nZVI has been reported as an effective remediation material for removal of heavy metal or organic pollutants, there are still many factors influencing its reactivity and stability, such as humic acid (HA) (Bhattacharjee and Ghoshal 2018b; Deng et al. 2020; Han et al. 2019), coexisting ions (Li et al. 2017a; Wang et al. 2020a), S/Fe molar ratio (Dong et al. 2018; Wu et al. 2018; Zhuang et al. 2021b), pH (Wu et al. 2019; Xu et al. 2020d; Zhang et al. 2020a), and oxygen condition (Du et al. 2016; Su et al. 2018; Tang et al. 2016). To further improve the applicability of S-nZVI, it is imperative to connect the influencing factors with the real application of S-nZVI, thereby achieving better remediation performance.

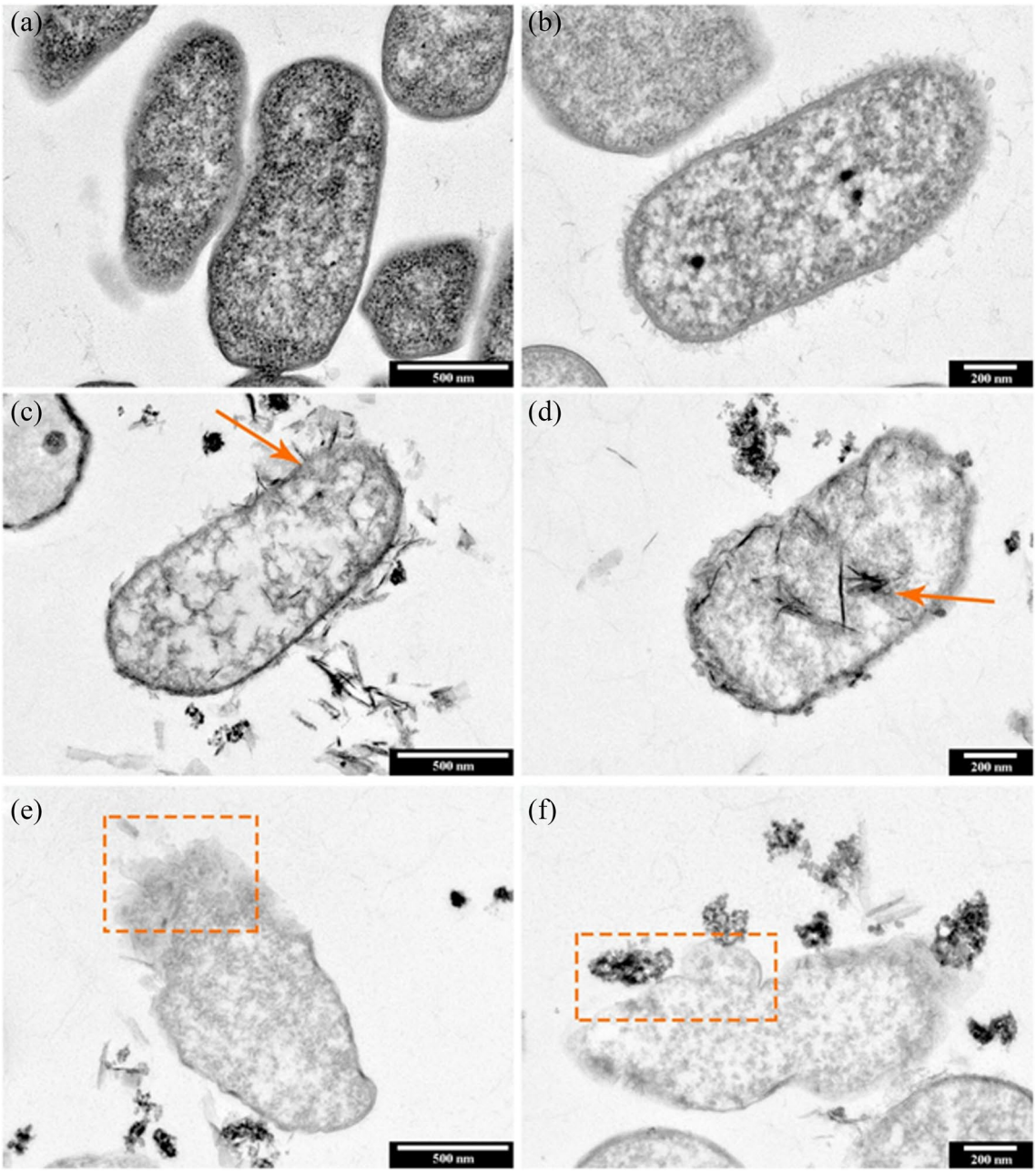

Fig. 10 TEM images of **a**, **b** untreated and **c**–**f** treated ARB cells in the supernatants (S-nZVI dosage, 1.12 g/L; S/Fe molar ratio, 0.1; initial ARB concentration, 2×10^7 CFU/mL; reaction time, 15 min). Reprinted with permission from Ref. (Wang et al. 2020b). Copyright 2020, Elsevier

Effect of humic acid

Previous studies have demonstrated that HA could enhance the dissolution of nZVI, increase its dispersion, and reduce its cytotoxicity through steric hindrance and electrostatic repulsion (Li et al. 2010). However, S-nZVI has different properties from nZVI, and HA contains active functional groups such as quinone, which have an affinity for iron and sulfur and may react with the FeS shell of S-nZVI (Liao et al. 2017). Therefore, exploring the impact of HA on S-nZVI is crucial for evaluating its performance. HA is one of the most prevalent natural organic matter in the environment and generally has a negative effect on the removal performance of S-nZVI towards specific pollutants in waters (Han et al. 2019; Xu et al. 2020d). Deng et al. (2020) found that the presence of HA would compete with Cr^{6+} for the active sites on the S-nZVI@BFS, thereby decreasing the removal rate

of S-nZVI@BFS for Cr^{6+}. Besides, the impact of HA on organic pollutants removal by S-nZVI has also been studied. Bhattacharjee and Ghoshal (2018b) found that the increased loading of HA largely decreased the TCE degradation efficiency by S-nZVI. It can be explained by two reasons: (1) the HA in the solution could adsorb part of TCE, reducing the TCE concentration on the S-nZVI surface and (2) the HA adsorbed onto S-nZVI blocked the active sites of TCE. Han et al. (2019) proposed that the addition of Suwannee River humic acid (SRHA) increased the dispersion stability and surface negative charge of S-nZVI, but also promoted the corrosion of S-nZVI particles. The SRHA being adsorbed on the surface of S-nZVI contributed to the dissolution of FeS and the generation of passivation film, which also decreased the reactivity of S-nZVI to TCE. When the concentration of SRHA was 200 mg C/L, the rate constant of TCE degradation in groundwater by S-nZVI decreased by 60%, and with the increase of SRHA dosage, the inhibitory effect of SRHA on the reactivity of S-nZVI was more potent. Therefore, it is necessary to carefully consider the stability of S-nZVI in the existence of HA, especially the long-term effect of HA on the integrity of FeS shells on S-nZVI while applying S-nZVI for groundwater remediation.

Effect of coexisting ions

Inorganic anions (e.g., HPO_4^{2-}, PO_4^{2-}, NO_3^-, HCO_3^-, and Cl^-) typically affected the decontamination performance of S-nZVI by occupying the reactive sites due to different affinity with iron species and intrinsic characteristics. For example, Wu et al. (2018) investigated the impact of HPO_4^{2-} on S-nZVI for removal of As. Due to the fact that P and As had comparable chemical characteristics and ion sizes, HPO_4^{2-} could compete with As for active sites on the surface of S-nZVI. Deng et al. (2020) found that phosphate (PO_4^{3-}) could form precipitation with iron species and occupy the active sites on the surface of S-nZVI@BFS, thereby decreasing its reactivity with Cr^{6+}. Moreover, the NO_3^- as a strong oxidant could compete reduction sites with Cr^{6+}, thereby decreasing the removal efficiency of S-nZVI@BFS for Cr^{6+}. However, the existence of NO_3^- could facilitate the TCE degradation by S-nZVI, such a phenomenon occurs for the reason that NO_3^- as an oxidant was reduced by S-nZVI producing reducing hydrogen and Fe^{2+} (Wang et al. 2020a). Li et al. (2017a) found that both HCO_3^- and Cl^- had a detrimental influence on the degradation of hexabromocyclododecane (HBCD) due to their affinity with iron species. However, it was also revealed that NO_3^- had the largest adverse effect on the HBCD transformation due to its strong oxidizing properties. Inorganic cations usually complex with Fe or S species thus influencing the reactivity of S-nZVI. For example, Wang et al. (2020a) observed that the existence of Cr^{6+} and Cd^{2+} would result in the inhibition of S-nZVI to TCE removal, which was not only due to the generation of Fe–Cr hydroxides or Fe-Cd hydroxides, but also the concurrent reduction of Cr^{6+} to Cr^{3+}.

Effect of S/Fe molar ratio

The S/Fe molar ratio is an important parameter for pollutant removal and proper increase of S/Fe could increase the active sites and improve the surface activity of S-nZVI, thereby facilitating pollutants removal by S-nZVI (Dong et al. 2018; Song et al. 2023; Wu et al. 2018). The formation of FeS could increase the surface area, reactivity, and electron transfer of S-nZVI. Moreover, the S^{2-} from FeS could also form insoluble precipitation with metallic ions, such as Cd^{2+} and Pb^{2+} (Lv et al.2018; Song et al. 2023). Generally, the pollutants removal efficiencies generally increased first and then dropped as the S/Fe molar ratio increased. However, the high S/Fe molar ratio with excessive S would decrease the pollutants removal efficiency due to the formation of FeS_n, which could block the active sites and inhibit the electron shuttle (Dong et al. 2018; Zhuang et al. 2021b). Zhang et al. (2020a) reported that S-nZVI@BC with S/Fe molar ratio of 0.2 displayed the highest adsorption capacity for TBBPA. However, the generation of secondary FeS precipitates at high S/Fe molar ratio would prevent the Fe^0 from corrosion, thus restraining the TBBPA removal. Li et al. (2021b) demonstrated that the highest removal efficiency of S-nZVI/DMSN for TBBPA was obtained at the S/Fe molar ratio of 0.1 and a significant decrease of TBBPA removal efficiency was observed as the S/Fe molar ratio increased to 0.3. A proper S/Fe molar ratio enhanced electron transfer efficiency by connecting FeS and Fe^0 fully and effectively, while the overhigh S/Fe molar ratio could inhibit the pollutants removal by consuming abundant Fe^0 forming FeS_n, which was less reactive compared with FeS. However, some studies showed that higher S content could facilitate the pollutants removal. Li et al. (2016) proposed that the transformation rates of TBBPA and the concentration of final debrominated products increased with the S/Fe molar ratio increasing from 0.12 to 0.51, which may be attributed to the increased surface area of the S-nZVI with higher S/Fe molar ratio. Wu et al. (2018) proposed that the S content and surface roughness of S-nZVI increased as the S/Fe molar ratio rose from 0 to 0.35, and high S content would provide more binding sites for As.

Effect of pH

The reactivity of nZVI was easily prone to be affected by the fluctuation of pH and the impact of solution pH on the

pollutants removal rate was not negligible (Dong et al. 2018). The sulfuration largely enhanced the stability and reactivity of nZVI in alkaline environment, making its pH range of application more widely (Su et al. 2020). It was observed that the degradation efficiency of S-nZVI for TCE maintained at 90% after reacting for 9 h with pH ranging from 5 to 9 (Dong et al. 2018). Generally speaking, under acidic conditions, pH would improve the removal performance of S-nZVI for pollutants. Zhang et al. (2020a). proposed that the removal of S-Fe^0/BC for TBBPA was favored under acidic condition due to the enhanced electron transfer, in which adequate H^+ can destroy the passivation layer. However, the TBBPA removal was inhibited in extremely acidic situation due to the formation of hydrogen, which consumed electrons as well as decreased the connection between S-nZVI and TBBPA. Moreover, the iron hydroxides precipitates are prone to form under alkaline condition, which would decrease the reactivity of S-nZVI for pollutants. Li et al. (2021b) observed that the degradation efficiency of S-nZVI/DMSN for TBBPA dropped from 57 to 36.1% with pH increasing from 9 to 11. The Fe^{2+} produced from the oxidization of Fe^0 could combine with hydroxide ions forming iron hydroxides, which inhibited the connect between S-nZVI/DMSN and target pollutants. Zhang et al. (2020a) also found that the adsorption capacity of TBBPA by S-Fe^0/BC decreased from 1.47 to 0.77 mg/g as the pH rose from 8 to 11. It was proposed that the removal of S-nZVI for TBBPA was hindered under alkaline condition due to the formation of iron hydroxides precipitates, which occupied the reactive sites on the surface of S-Fe^0/BC.

Effect of oxygen condition

Oxygen condition is also a key factor affecting the effectiveness of S-nZVI during the process of environmental remediation. The impacts of dissolved oxygen on the pollutant removal by S-nZVI are different in different pathways. Tang et al. (2016) found that S-nZVI had different degradation pathways towards ρ-nitrophenol (PNP) with the change of oxygen condition. In anoxic stage, the PNP was reduced into ρ-aminophenol by atomic hydrogen. In aerobic stage, the PNP was oxidized into acetic acid by ·OH. When the mechanism for removing pollutants by S-nZVI is reduction, the dissolved oxygen can inhibit the removal of S-nZVI. While oxidization is responsible for the pollutant removal by S-nZVI, the removal process is facilitated by the dissolved oxygen (Dong et al. 2018; Song et al. 2017). Based on this, Wu et al. (2019) invented a sequential anoxic/oxic process for complete degradation of TBBPA by S-nZVI. In the anoxic stage, TBBPA was entirely converted to bisphenol A (BPA) through a four-step sequential debromination route, and S-nZVI inhibited H_2 precipitation, preserving the reductive capacity of Fe(0). In the oxidation stage, the resultant BPA was attacked by ·OH, converted to dihydroxybenzene and benzoquinone, and finally mineralized through ring-opening reactions. The sulfuration process promotes the formation of ·OH through surface-bound Fe(II) via a dual electron transport pathway, in which the structures Fe(II) and Fe(0) in FeS reduce Fe(III) to generate regenerated Fe(II), which plays a crucial part in the total degradation of BPA (Fig. 11). The study demonstrated the feasibility of

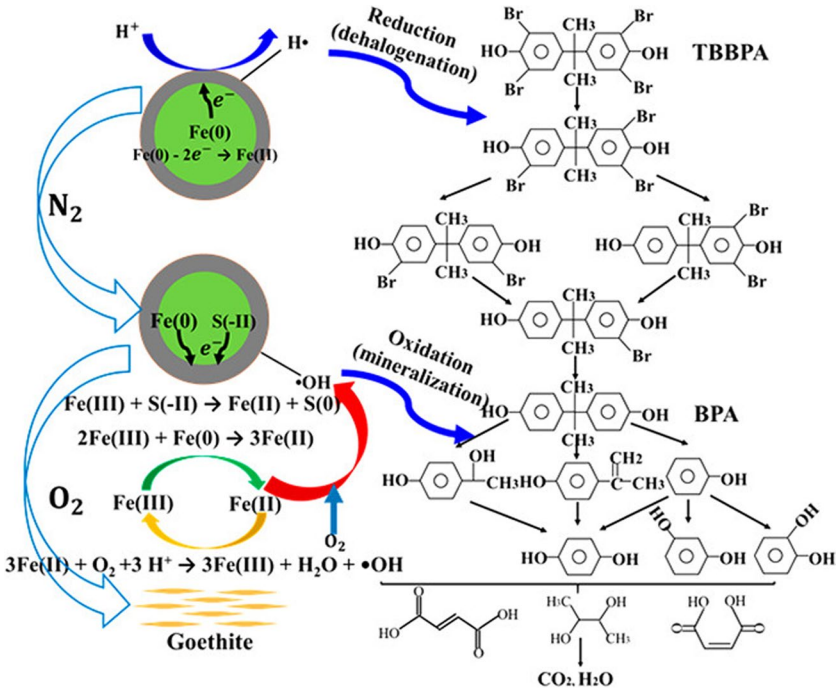

Fig. 11 Proposed pathways for TBBPA degradation by S-nZVI in the dynamic two-step anoxic/oxic process. Reprinted with permission from Ref. (Wu et al. 2019). Copyright 2019, American Chemical Society

complete degradation of refractory pollutants in a dynamic anoxic/oxic process, thereby expanding the environmental application of S-nZVI in water treatment.

Some studies revealed that dissolved oxygen could compete with pollutants for electrons donated by S-nZVI, thus decreasing the reduction power of S-nZVI towards Cr^{6+}. Du et al. (2016) proposed that the removal rate of S-nZVI for Cr^{6+} was restrained in the oxic situation, and the reason was that the dissolved oxygen could not only compete the electrons with Cr^{6+} but also react with Fe^{2+}. Similarly, it was also demonstrated that the removal capacity of S-nZVI@BC for Cr^{6+} was slightly increased under anaerobic situation than that under aerobic situation (Gao et al. 2018).

Based on such discussion, it can be seen that the effect of various environmental parameters on the S-nZVI is non-negligible. Accordingly, it is necessary to study such factors for optimal operation condition of S-nZVI.

Application of S-nZVI in advanced oxidation processes

AOP, as a novel technology, is of increasing interest for the high removal efficiency towards refractory pollutants with the formation of highly reactive oxidizing species (ROS, e.g., $SO_4^{-\cdot}$, ·OH, ·OOH, and $^1O_2$) (Wu et al. 2022a). Recent studies show that $SO_4^{-\cdot}$ is more adaptable for remediation due to some characteristics, such as stronger selectivity, higher redox potential, longer half-life, higher selectivity, and wider pH application range (Kang et al. 2018b; Wu et al. 2022a). Besides, PS, including peroxymonosulfate (PMS) and peroxydisulfate (PDS), has become popular for its strong stability and high reactivity as compared to the traditional oxidants (e.g., peroxide and permanganate) toward pollutants (Dong et al. 2019a).

In the sulfate-based AOP, Fe^{2+}, as a catalyst, combined with PS, has been applied to eliminate pollutants (Chen et al. 2020). In the Fe^{2+}/PMS system, the Fe^{2+} could react with PMS forming Fe^{3+} and reactive $SO_4^{-\cdot}$ and the generated Fe^{3+} could further react with PMS forming $SO_5^{-\cdot}$ (Eq. (20)-(21)). Besides, the reaction between $SO_4^{-\cdot}$ and OH^- could also produce highly reactive ·OH radicals (Eq. (22)) (Liu et al. 2022b). In the Fe^{2+}/PDS system, the formation of $SO_4^{-\cdot}$ could be achieved via the reaction between Fe^{2+} and $S_2O_8^{2-}$ (Eq. (23)) (Wu et al. 2022a). Some researchers proposed that the quantity of Fe^{2+} is vital to the reaction performance of sulfate-based AOP. The system with a small number of Fe^{2+} is less reactive, whereas excessive Fe^{2+} could react with the sulfate radicals in which the formation rate is less than the elimination rate and even compete with pollutants over limited electrons, leading to the decline of oxidative potential and removal efficiency (Chen et al. 2020; Kang et al. 2018b; Wu et al. 2022a). nZVI, as a solid-phase catalyst, can be a good alternative to Fe^{2+}, for which releases Fe^{2+} slowly retaining a controlled Fe^{2+} concentration. Moreover, the combination of nZVI and PS has been proved effective for removal of various pollutants. For example, Yan et al. (2015) proposed that the degradation efficiency of TCE by nZVI@BC composite activated PS can reach up to 99.4%. Song et al. (2022) demonstrated that the SMX degradation efficiency can obtain 98.6% by nZVI activated PDS with the existence of Molybdenum disulfide as a co-catalyst. However, the application of nZVI was limited due to its inherent characteristics, such as easy to be oxidized and susceptible to agglomeration. Therefore, S-nZVI can be an alternative or an improved version to nZVI for its intrinsic properties.

$$Fe^{2+} + HSO_5^- \rightarrow Fe^{3+} + SO_4^{-\cdot} + OH^- \quad (20)$$

$$Fe^{3+} + HSO_5^- \rightarrow Fe^{2+} + SO_5^{-\cdot} + H^+ \quad (21)$$

$$SO_4^{-\cdot} + OH^- \rightarrow \cdot OH + SO_4^{2-} \quad (22)$$

$$Fe^{2+} + S_2O_8^{2-} \rightarrow SO_4^{-\cdot} + Fe^{3+} + SO_4^{2-} \quad (23)$$

Recently, S-nZVI/PS has been utilized for the removal of organic pollutants. For instance, Cai and Zhang (2022) found that in comparison with the nZVI/PS system (0.089 min^{-1}), the S-nZVI/PS system had a greater degradation activity for bisphenol S (BPS) (0.142 min^{-1}), especially at high BPS concentrations. The FeS_x layer could improve the passivation and aggregation of nZVI, enhance electron transfer, and improve the activation performance of nZVI on PS. $SO_4^{-\cdot}$ and ·OH were the main oxidants for degrading BPS. In addition, BPS could be effectively removed within a wide initial pH range (3.13–9.35). S-nZVI has proved to be effective for the elimination of antibiotics. The removal efficiency of SMX by S-nZVI coupled PS was 97.5%, and the removal process was in good conformity with the pseudo-first-order kinetics model. Both ·OH and $SO_4^{-\cdot}$ were responsible for the SMX removal, and $SO_4^{-\cdot}$ served as the main free radical (Yu et al. 2022b). In other studies, it was observed that the removal efficiency of S-nZVI/PS for TC and CAP could achieve 93.8% and 98.8%, respectively, (Yu et al. 2022a, 2022b).

In the context of remediation, the ROS generated from S-nZVI@PS could inactivate the ARB and eliminate the ARGs (Yu et al. 2021). Yu et al. (2021) used S-nZVI coupling PS to simultaneously remove ARB and ARGs. The complete inactivation of S-nZVI/PS for ARB was achieved within 10 min (~7.8 log decreased) and degraded all eARGs within 5 min (~8.0 log decreased) (Fig. 12a–d). In addition, S-nZVI/PS could also complete the deactivation of ARB in real drinking water and wastewater containing NOM

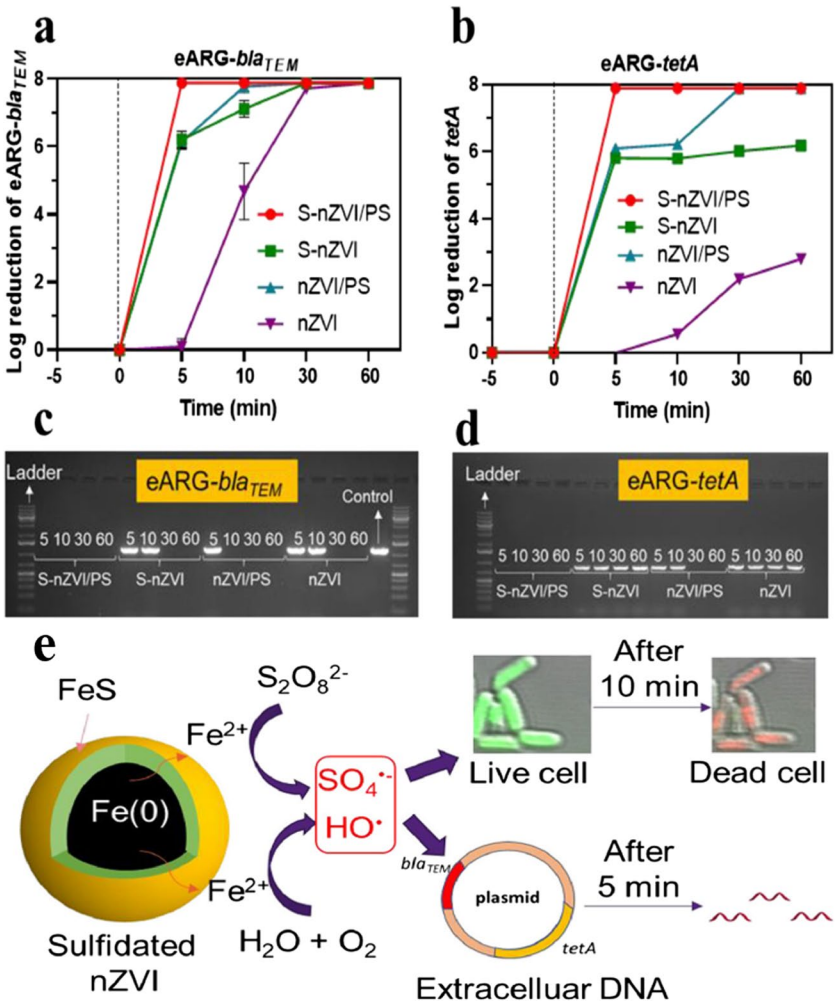

Fig. 12 **a**, **b** Degradation of extracellular antibiotic resistance genes (eARGs) with different particles treatment. **c**, **d** Log reduction of eARGs (bla_{TEM} and *tetA*) under different treatment and their corresponding gel electrophoresis images. **e** Removal mechanisms of ARGs and ARB by S-nZVI/PS. Reprinted with permission from Ref. (Yu et al. 2021). Copyright 2021, Elsevier

and suspended solids. It can be seen from the regeneration experiment that the treated ARB was disappeared after 72 h or more of incubation, indicating that the permanent inactivation of ARB by $SO_4^{-\cdot}$ and ·OH radicals occurred (Fig. 12e). Also, S-nZVI was found to be efficient PMS or PDS activator. Liu et al. (2022b) proposed that S-nZVI/PMS system had better deactivation effect on ARB than S-nZVI/PDS system. In the low concentration S-nZVI/PMS system, ARB cells typically reduce by approximately 7.32 logs (effective inactivation) within 15 min. At the same time, because of oxidative stress and lipid peroxidation, the structural integrity (cell wall and membrane) of ARB cells was severely damaged, leading to damage and leakage of genetic material within the cells. The collaborative S-nZVI/PS system is expected to be used for water purification, including inactivation of ARB and degradation of related ARGs, thereby restricting the propagation of antibiotic resistance in the actual environment. Future studies of up-scaling investigations and the effect of other water quality parameters, including pH, suspended solids, and turbidity, on removal of ARBs and ARGs are needed.

The environmental toxicity of S-nZVI

It has been reported that nZVI itself has toxicity to some content towards microorganisms. The Fe^{2+} released from nZVI and the generated ROS could cause damage to the microorganism. Similarly, the application of S-nZVI could also cause toxic effect on the microorganism in the environment.

Some researchers proposed that S-nZVI was less toxic than nZVI (Cheng et al. 2019; Han et al. 2019). For example, Han et al. (2019) proposed that the sulfidation of nZVI slightly alleviated the toxicity to *E. coli*. and the *E. coli*. culturability maintained around 20% after being exposed to S-nZVI for 4 h. The remained toxicity was ascribed to the increased surface area and dispersion of S-nZVI compared with bare nZVI. Cheng et al. (2019) investigated the source of toxicity of S-nZVI towards *E. coli* and demonstrated that the ROS produced by the oxidization of Fe^0 played a vital role in destructing the integrity of cell membrane and further inactivating the cell. They also studied many influencing factors related to the toxicity of S-nZVI, such as Fe/S ratio, typical groundwater components, and particle

aging. It was found that S-nZVI with low toxicity could be achieved at a lower Fe/S molar ratio, the existence of groundwater component can decrease the toxicity of S-nZVI to some extent and the toxicity of S-nZVI would decrease with the aging time. Besides, it is also necessary to explore appropriate methods to assess the toxicity of S-nZVI. Semerád et al. (2020) assessed the toxicity of S-nZVI through oxidative stress assay based on lipid peroxidation and found that higher stability and lower toxicity could be achieved with the increase of S content. However, the S-nZVI particles aging for 7 days performed similar oxidative stress with nZVI. In this way, it is also imperative to study the toxicity of aging S-nZVI.

Accordingly, S-nZVI may be a good alternative to nZVI with higher applicability. It can be concluded that the toxicity mechanisms of S-nZVI may be a combination of ROS and nano-specific Fe^{2+} toxicity. The measures for alleviating the toxic effect of S-nZVI is dependent on restraining the direct contact between S-nZVI and microorganism.

Challenge and perspective

Though S-nZVI is a good decontamination material, there are still some restrains and knowledge gaps imperative for further study, which is essential for further advancing the development of S-nZVI-based remediation technology. Some points are listed as follows:

(1) As to the synthesis method of S-nZVI, the chemical reduction method is the most common method due to its easy operation and high efficiency. However, the reduction agent borohydride used to prepare Fe^0 particles is relatively expensive. Moreover, the formed H_2S is toxic and further decreases the incorporated sulfur content of S-nZVI. Therefore, it is necessary to explore more economic and benign synthesis methods for higher applicability of S-nZVI.

(2) The role of FeS_x shell of S-nZVI on the decontamination performance has been demonstrated by many research. However, the sulfur transformation in the content and distribution during the removal process of pollutants should also be considered.

(3) Some studies revealed that the decontamination performance of S-nZVI is not always superior to nZVI. Moreover, the information on the effect of sulfidation time on the decontamination performance of S-nZVI is limited. In this way, it is imperative to investigate the role of sulfidation time play and conduct more comparative experiments over nZVI and S-nZVI to further improve the role of sulfidation.

(4) The removal of pollutants by S-nZVI always focuses on the parent pollutants, while the partially decontaminated intermediate products are easily ignored. Consequently, it may bring about higher cost input and lower remediation effect. Therefore, it is urgent to analyze the reaction products and achieve better remediation performance.

(5) S-nZVI has good immobilization performance for metallic ions and degradation efficiency for organic compounds. However, there is limited information on the remediation efficiency and removal mechanisms of S-nZVI toward complex environment with multiple pollutants involved. Therefore, it is of significant importance to assess the applicability and explore the remediation pathway of S-nZVI.

(6) At present, most studies on the removal performance of S-nZVI are confined to the laboratory experiment. However, the field parameter is complex and inconstant. Therefore, field remediation of contaminated sites is needed for further studying the optimal environmental factors to remove specific pollutants in the proper condition. Moreover, the effect of the addition of S-nZVI on the environmental matrix and the effect of field condition on the fate and transport of S-nZVI should also be further investigated.

(7) Sulfate-based AOP technology is a promising remediation method by taking advantage of oxidative capacity endowed by formed ROS. However, some studies demonstrated that the selectivity of ROS is not so good for application, while the non-radical has higher selectivity and is more adaptable for application. Moreover, the combination of multiple AOP has been reported to produce more ROS than sole AOP. In this way, it is critical to compare the remediation efficiency of radical and non-radical and explore whether there is an optimal combination AOP for further improvement of the remediation efficiency of sulfate-based AOP.

(8) Sulfidation of nZVI largely increase its reactivity and selectivity, while the toxicity of S-nZVI restrains its further scale-up application. By now, the research on the toxicity of nZVI is more than that of S-nZVI. Meanwhile, some measures have been proposed to alleviate the toxicity of nZVI whereas limited counterparts for S-nZVI. Accordingly, there is an urgent need to study the toxicity mechanism of S-nZVI and develop corresponding measures to enhance its biocompatibility.

Author contribution Wenjing Xue: conceptualization, writing—review and editing, writing—original draft, and funding acquisition. Jun Li: supervision, writing—review and editing, and writing—original draft. Xinyu Chen, Hongdou Liu, Siqi Wen, Xiaoyu Shi, Jiaming Guo, Yang Gao, and Jian Xu: review and editing. Yiqun Xu: conceptualization, methodology, and writing—review and editing.

Funding This work was financially supported by the Program for the National Natural Science Foundation of China (42107415) and Natural Science Foundation of Jiangsu Province (BK20210830).

Data availability The data analyzed and/or generated in this study are available upon reasonable request from the corresponding author.

Declarations

Ethical approval This is not applicable.

Consent to participate This is not applicable.

Consent to publish This is not applicable.

Competing interests The authors declare no competing interests.

References

Ainiwaer M, Zhang T, Zhang N, Yin X, Su S, Wang Y, Zhang Y, Zeng X (2022) Synergistic removal of As(III) and Cd(II) by sepiolite-modified nanoscale zero-valent iron and a related mechanistic study. J Environ Manag 319:115658. https://doi.org/10.1016/j.jenvman.2022.115658

Bae S, Collins RN, Waite TD, Hanna K (2018) Advances in surface passivation of nanoscale zerovalent iron: a critical review. Environ Sci Technol 52:12010–12025. https://doi.org/10.1021/acs.est.8b01734

Baldermann A, Kaufhold S, Dohrmann R, Baldermann C, Letofsky-Papst I, Dietzel M (2021) A novel nZVI-bentonite nanocomposite to remove trichloroethene (TCE) from solution. Chemosphere 282:131018. https://doi.org/10.1016/j.chemosphere.2021.131018

Bhattacharjee S, Ghoshal S (2018a) Optimal design of sulfidated nanoscale zerovalent iron for enhanced trichloroethene degradation. Environ Sci Technol 52:11078–11086. https://doi.org/10.1021/acs.est.8b02399

Bhattacharjee S, Ghoshal S (2018b) Sulfidation of nanoscale zerovalent iron in the presence of two organic macromolecules and its effects on trichloroethene degradation. Environ Sci Nano 5:782–791. https://doi.org/10.1039/c7en01205e

Bin Q, Lin B, Zhu K, Shen Y, Man Y, Wang B, Lai C, Chen W (2020) Superior trichloroethylene removal from water by sulfide-modified nanoscale zero-valent iron/graphene aerogel composite. J Environ Sci 88:90–102. https://doi.org/10.1016/j.jes.2019.08.011

Brumovský M, Filip J, Malina O, Oborná J, Sracek O, Reichenauer TG, Andrýsková P, Zbořil R (2020) Core-shell Fe/FeS nanoparticles with controlled shell thickness for enhanced trichloroethylene removal. ACS Appl Mater Interfaces 12:35424–35434. https://doi.org/10.1021/acsami.0c08626

Brumovský M, Oborná J, Lacina P, Hegedüs M, Sracek O, Kolařík J, Petr M, Kašlík J, Hofmann T, Filip J (2021) Sulfidated nanoscale zerovalent iron is able to effectively reduce in situ hexavalent chromium in a contaminated aquifer. J Hazard Mater 405:124665. https://doi.org/10.1016/j.jhazmat.2020.124665

Cai J, Zhang Y (2022) Enhanced degradation of bisphenol S by persulfate activated with sulfide-modified nanoscale zero-valent iron. Environ Sci Pollut Res Int 29:8281–8293. https://doi.org/10.1007/s11356-021-16156-8

Cao Z, Liu X, Xu J, Zhang J, Yang Y, Zhou J, Xu X, Lowry GV (2017) Removal of antibiotic florfenicol by sulfide-modified nanoscale zero-valent iron. Environ Sci Technol 51:11269–11277. https://doi.org/10.1021/acs.est.7b02480

Cao Z, Xu J, Li H, Ma T, Lou L, Henkelman G, Xu X (2020) Dechlorination and defluorination capability of sulfidized nanoscale zerovalent iron with suppressed water reactivity. Chem Eng J 400:125900. https://doi.org/10.1016/j.cej.2020.125900

Cao Z, Li H, Lowry GV, Shi X, Pan X, Xu X, Henkelman G, Xu J (2021) Unveiling the role of sulfur in rapid defluorination of florfenicol by sulfidized nanoscale zero-valent iron in water under ambient conditions. Environ Sci Technol 55:2628–2638. https://doi.org/10.1021/acs.est.0c07319

Chen R, Yin H, Peng H, Wei X, Yu X, Xie D, Lu G, Dang Z (2020) Removal of triphenyl phosphate by nanoscale zerovalent iron (nZVI) activated bisulfite: performance, surface reaction mechanism and sulfate radical-mediated degradation pathway. Environ Pollut 260:113983. https://doi.org/10.1016/j.envpol.2020.113983

Chen M, Xu H, Zhang Y, Zhao X, Chen Y, Kong X (2022) Effective removal of heavy metal ions by attapulgite supported sulfidized nanoscale zerovalent iron from aqueous solution. Colloids Surf A Physicochem Eng Asp 640:128192. https://doi.org/10.1016/j.colsurfa.2021.128192

Cheng Y, Dong H, Lu Y, Hou K, Wang Y, Ning Q, Li L, Wang B, Zhang L, Zeng G (2019) Toxicity of sulfide-modified nanoscale zero-valent iron to Escherichia coli in aqueous solutions. Chemosphere 220:523–530. https://doi.org/10.1016/j.chemosphere.2018.12.159

Cheng Y, Yang S, Yin L, Pu Y, Liang G (2023) Recent consequences of micro-nanaoplastics (MNPLs) in subcellular/molecular environmental pollution toxicity on human and animals. Ecotoxicol Environ Saf 249:114385. https://doi.org/10.1016/j.ecoenv.2022.114385

Chi Z, Ju S, Liu X, Sun F, Zhu Y (2022) Graphene oxide supported sulfidated nano zero-valent iron (S-nZVI@GO) for antimony removal: the role of active oxygen species and reaction mechanism. Chemosphere 308:136253. https://doi.org/10.1016/j.chemosphere.2022.136253

Crane RA, Scott TB (2012) Nanoscale zero-valent iron: future prospects for an emerging water treatment technology. J Hazard Mater 211–212:112–125. https://doi.org/10.1016/j.jhazmat.2011.11.073

Daneshkhah M, Hossaini H, Malakootian M (2017) Removal of metoprolol from water by sepiolite-supported nanoscale zero-valent iron. J Environ Chem Eng 5:3490–3499. https://doi.org/10.1016/j.jece.2017.06.040

Deng M, Wang X, Li Y, Wang F, Jiang Z, Liu Y, Gu Z, Xia S, Zhao J (2020) Reduction and immobilization of Cr(VI) in aqueous solutions by blast furnace slag supported sulfidized nanoscale zerovalent iron. Sci Total Environ 743:140722. https://doi.org/10.1016/j.scitotenv.2020.140722

Devi P, Dalai AK (2019) Effects of carboxymethyl cellulose grafting on stability and reactivity of zerovalent iron in water systems. J Clean Prod 229:65–74. https://doi.org/10.1016/j.jclepro.2019.04.364

Dong H, Zhang C, Hou K, Cheng Y, Deng J, Jiang Z, Tang L, Zeng G (2017) Removal of trichloroethylene by biochar supported nanoscale zero-valent iron in aqueous solution. Sep Purif Technol 188:188–196. https://doi.org/10.1016/j.seppur.2017.07.033

Dong H, Zhang C, Deng J, Jiang Z, Zhang L, Cheng Y, Hou K, Tang L, Zeng G (2018) Factors influencing degradation of trichloroethylene by sulfide-modified nanoscale zero-valent iron in aqueous solution. Water Res 135:1–10. https://doi.org/10.1016/j.watres.2018.02.017

Dong H, Hou K, Qiao W, Cheng Y, Zhang L, Wang B, Li L, Wang Y, Ning Q, Zeng G (2019a) Insights into enhanced removal of TCE utilizing sulfide-modified nanoscale zero-valent iron activated persulfate. Chem Eng J 359:1046–1055. https://doi.org/10.1016/j.cej.2018.11.080

Dong H, Wang B, Li L, Wang Y, Ning Q, Tian R, Li R, Chen J, Xie Q (2019b) Activation of persulfate and hydrogen peroxide by using sulfide-modified nanoscale zero-valent iron for oxidative degradation of sulfamethazine: a comparative study. Sep Purif Technol 218:113–119. https://doi.org/10.1016/j.seppur.2019.2.052

Dong J, Li G, Gao J, Zhang H, Bi S, Liu S, Liao C, Jiang G (2022) Catalytic degradation of brominated flame retardants in the environment: new techniques and research highlights. Sci Total Environ 848:157695. https://doi.org/10.1016/j.scitotenv.2022.157695

Du J, Bao J, Lu C, Werner D (2016) Reductive sequestration of chromate by hierarchical FeS@Fe(0) particles. Water Res 102:73–81. https://doi.org/10.1016/j.watres.2016.06.009

Ezzatahmadi N, Ayoko GA, Millar GJ, Speight R, Yan C, Li J, Li S, Zhu J, Xi Y (2017) Clay-supported nanoscale zero-valent iron composite materials for the remediation of contaminated aqueous solutions: a review. Chem Eng J 312:336–350. https://doi.org/10.1016/j.cej.2016.11.154

Fan WK, Tahir M (2022) Structured clay minerals-based nanomaterials for sustainable photo/thermal carbon dioxide conversion to cleaner fuels: a critical review. Sci Total Environ 845:157206. https://doi.org/10.1016/j.scitotenv.2022.157206

Fan D, Anitori RP, Tebo BM, Tratnyek PG, Lezama Pacheco JS, Kukkadapu RK, Engelhard MH, Bowden ME, Kovarik L, Arey BW (2013) Reductive sequestration of pertechnetate (^{99}TcO4-) by nano zerovalent iron (nZVI) transformed by abiotic sulfide. Environ Sci Technol 47:5302–5310. https://doi.org/10.1021/es304829z

Fan D, Anitori RP, Tebo BM, Tratnyek PG, Lezama Pacheco JS, Kukkadapu RK, Kovarik L, Engelhard MH, Bowden ME (2014) Oxidative remobilization of technetium sequestered by sulfide-transformed nano zerovalent iron. Environ Sci Technol 48:7409–7417. https://doi.org/10.1021/es501607s

Fan D, Lan Y, Tratnyek PG, Johnson RL, Filip J, O'Carroll DM, Garcia AN, Agrawal A (2017) Sulfidation of iron-based materials: a review of processes and implications for water treatment and remediation. Environ Sci Technol 51:13070–13085. https://doi.org/10.1021/acs.est.7b04177

Foroughi M, Khiadani M, Kakhki S, Kholghi V, Naderi K, Yektay S (2022) Effect of ozonation-based disinfection methods on the removal of antibiotic resistant bacteria and resistance genes (ARB/ARGs) in water and wastewater treatment: a systematic review. Sci Total Environ 811:151404. https://doi.org/10.1016/j.scitotenv.2021.151404

Fu R, Yang Y, Xu Z, Zhang X, Guo X, Bi D (2015) The removal of chromium (VI) and lead (II) from groundwater using sepiolite-supported nanoscale zero-valent iron (S-NZVI). Chemosphere 138:726–734. https://doi.org/10.1016/j.chemosphere.2015.07.051

Fu T, Zhang B, Gao X, Cui S, Guan C, Zhang Y, Zhang B, Peng Y (2023) Recent progresses, challenges, and opportunities of carbon-based materials applied in heavy metal polluted soil remediation. Sci Total Environ 856:158810. https://doi.org/10.1016/j.scitotenv.2022.158810

Gao J, Yang L, Liu Y, Shao F, Liao Q, Shang J (2018) Scavenging of Cr(VI) from aqueous solutions by sulfide-modified nanoscale zero-valent iron supported by biochar. J Taiwan Inst Chem Eng 91:449–456. https://doi.org/10.1016/j.jtice.2018.06.033

Gao J, Han D, Xu Y, Liu Y, Shang J (2020) Persulfate activation by sulfide-modified nanoscale iron supported by biochar (S-nZVI/BC) for degradation of ciprofloxacin. Sep Purif Technol 235:116202. https://doi.org/10.1016/j.seppur.2019.116202

Gao F, Ahmad S, Tang J, Zhang C, Li S, Yu C, Liu Q, Sun H (2022a) Enhanced nitrobenzene removal in soil by biochar supported sulfidated nano zerovalent iron: solubilization effect and mechanism. Sci Total Environ 826:153960. https://doi.org/10.1016/j.scitotenv.2022.153960

Gao R, Hu P, Dai Y, Zhang Y, Liu L, Yang W (2022b) Removal of cadmium(II) from aqueous solutions by a novel sulfide-modified nanoscale zero-valent iron supported on kaolinite: treatment efficiency, kinetics and mechanisms. Appl Surf Sci 602:154353. https://doi.org/10.1016/j.apsusc.2022.154353

Gao F, Lyu H, Ahmad S, Xu S, Tang J (2023) Enhanced reductive degradation of tetrabromobisphenol A by biochar supported sulfidated nanoscale zero-valent iron: selectivity and core reactivity. Appl Catal B Environ 324:122246. https://doi.org/10.1016/j.apcatb.2022.122246

Garcia AN, Boparai HK, Chowdhury AIA, de Boer CV, Kocur CMD, Passeport E, Lollar BS, Austrins LM, Herrera J, O'Carroll DM (2020a) Sulfidated nano zerovalent iron (S-nZVI) for in situ treatment of chlorinated solvents: a field study. Water Res 174:115594. https://doi.org/10.1016/j.watres.2020.115594

Garcia AN, Boparai HK, de Boer CV, Chowdhury AIA, Kocur CMD, Austrins LM, Herrera J, O'Carroll DM (2020b) Fate and transport of sulfidated nano zerovalent iron (S-nZVI): a field study. Water Res 170:115319. https://doi.org/10.1016/j.watres.2019.115319

Gong Y, Gai L, Tang J, Fu J, Wang Q, Zeng E (2017) Reduction of Cr(VI) in simulated groundwater by FeS-coated iron magnetic nanoparticles. Sci Total Environ 595:743–751. https://doi.org/10.1016/j.scitotenv.2017.03.282

Gong L, Shi S, Lv N, Xu W, Ye Z, Gao B, O'Carroll DM, He F (2020) Sulfidation enhances stability and mobility of carboxymethyl cellulose stabilized nanoscale zero-valent iron in saturated porous media. Sci Total Environ 718:137427. https://doi.org/10.1016/j.scitotenv.2020.137427

Gu Y, Wang B, He F, Bradley MJ, Tratnyek PG (2017) Mechanochemically sulfidated microscale zero valent iron: pathways, kinetics, mechanism, and efficiency of trichloroethylene dechlorination. Environ Sci Technol 51:12653–12662. https://doi.org/10.1021/acs.est.7b03604

Guan X, Yang H, Sun Y, Qiao J (2019) Enhanced immobilization of chromium(VI) in soil using sulfidated zero-valent iron. Chemosphere 228:370–376. https://doi.org/10.1016/j.chemosphere.2019.04.132

Guo Y, Li X, Liang L, Lin Z, Su X, Zhang W (2021) Immobilization of cadmium in contaminated soils using sulfidated nanoscale zero-valent iron: effectiveness and remediation mechanism. J Hazard Mater 420:126605. https://doi.org/10.1016/j.jhazmat.2021.126605

Haciosmanoğlu GG, Mejías C, Martín J, Santos JL, Aparicio I, Alonso E (2022) Antibiotic adsorption by natural and modified clay minerals as designer adsorbents for wastewater treatment: a comprehensive review. J Environ Manag 317:115397. https://doi.org/10.1016/j.jenvman.2022.115397

Han Y, Yan W (2016) Reductive dechlorination of trichloroethene by zero-valent iron nanoparticles: reactivity enhancement through sulfidation treatment. Environ Sci Technol 50:12992–13001. https://doi.org/10.1021/acs.est.6b03997

Han Y, Ghoshal S, Lowry GV, Chen J (2019) A comparison of the effects of natural organic matter on sulfidated and nonsulfidated nanoscale zerovalent iron colloidal stability, toxicity, and reactivity to trichloroethylene. Sci Total Environ 671:254–261. https://doi.org/10.1016/j.scitotenv.2019.03.343

Han Z, Salawu OA, Zenobio JE, Zhao Y, Adeleye AS (2021) Emerging investigator series: immobilization of arsenic in soil by nanoscale zerovalent iron: role of sulfidation and application of machine learning. Environ Sci Nano 8:619–633. https://doi.org/10.1039/d0en01202e

Harindintwali JD, He C, Xiang L, Dou Q, Liu Y, Wang M, Wen X, Fu Y, Islam MU, Chang S, Kueppers S, Shaheen SM, Rinklebe J, Jiang X, Schaeffer A, Wang F (2023) Effects of ball milling on biochar adsorption of contaminants in water: a

meta-analysis. Sci Total Environ 882:163643. https://doi.org/10.1016/j.scitotenv.2023.163643
He F, Li Z, Shi S, Xu W, Sheng H, Gu Y, Jiang Y, Xi B (2018) Dechlorination of excess trichloroethene by bimetallic and sulfidated nanoscale zero-valent iron. Environ Sci Technol 52:8627–8637. https://doi.org/10.1021/acs.est.8b01735
He Y, Li J, Zhao Y, Yang C, Xu C, Liu X, Xing X, Tie J, Li R, Zheng J (2022) Sewage-sludge derived activated carbon impregnated with polysulfide-sulfidated nZVI: a promising material for Cr (VI) reductive stabilization. Colloids Surf A Physicochem Eng Asp 642:128614. https://doi.org/10.1016/j.colsurfa.2022.128614
Huang D, Xue W, Zeng G, Wan J, Chen G, Huang C, Zhang C, Cheng M, Xu P (2016) Immobilization of Cd in river sediments by sodium alginate modified nanoscale zero-valent iron: impact on enzyme activities and microbial community diversity. Water Res 106:15–25. https://doi.org/10.1016/j.watres.2016.09.050
Jiang Q, Jiang S, Li H, Zhang R, Jiang Z, Zhang Y (2022) A stable biochar supported S-nZVI to activate persulfate for effective dichlorination of atrazine. Chem Eng J 431:133937. https://doi.org/10.1016/j.cej.2021.133937
Kang Y, Vu H, Le T, Chang Y (2018a) Activation of persulfate by a novel Fe(II)-immobilized chitosan/alginate composite for bisphenol A degradation. Chem Eng J 353:736–745. https://doi.org/10.1016/j.cej.2018.07.175
Kang Y, Yoon H, Lee W, Kim E, Chang Y (2018b) Comparative study of peroxide oxidants activated by nZVI: removal of 1,4-dioxane and arsenic(III) in contaminated waters. Chem Eng J 334:2511–2519. https://doi.org/10.1016/j.cej.2017.11.076
Kim E, Kim J, Azad AM, Chang Y (2011) Facile synthesis and characterization of Fe/FeS nanoparticles for environmental applications. ACS Appl Mater Interfaces 3:1457–1462. https://doi.org/10.1021/am200016v
Kong X, Xuan L, Fu Y, Yuan F, Qin C (2021) Effect of the modification sequence on the reactivity, electron selectivity, and mobility of sulfidated and CMC-stabilized nanoscale zerovalent iron. Sci Total Environ 793:148487. https://doi.org/10.1016/j.scitotenv.2021.148487
Kotchaplai P, Khan E, Vangnai AS (2017) Membrane alterations in pseudomonas putida F1 exposed to nanoscale zerovalent iron: effects of short-term and repetitive nZVI exposure. Environ Sci Technol 51:7804–7813. https://doi.org/10.1021/acs.est.7b00736
Lefevre E, Bossa N, Wiesner MR, Gunsch CK (2016) A review of the environmental implications of in situ remediation by nanoscale zero valent iron (nZVI): behavior, transport and impacts on microbial communities. Sci Total Environ 565:889–901. https://doi.org/10.1016/j.scitotenv.2016.02.003
Li Z, Greden K, Alvarez PJJ, Gregory KB, Lowry GV (2010) Adsorbed polymer and NOM limits adhesion and toxicity of nano scale zerovalent iron to *E. coli*. Environ Sci Technol 44:3462–3467. https://doi.org/10.1021/es9031198
Li D, Mao Z, Zhong Y, Huang W, Wu Y, Peng P (2016) Reductive transformation of tetrabromobisphenol A by sulfidated nano zerovalent iron. Water Res 103:1–9. https://doi.org/10.1016/j.watres.2016.07.003
Li D, Zhu X, Zhong Y, Huang W, Peng P (2017a) Abiotic transformation of hexabromocyclododecane by sulfidated nanoscale zerovalent iron: kinetics, mechanism and influencing factors. Water Res 121:140–149. https://doi.org/10.1016/j.watres.2017.05.019
Li J, Zhang X, Sun Y, Liang L, Pan B, Zhang W, Guan X (2017b) Advances in sulfidation of zerovalent iron for water decontamination. Environ Sci Technol 51:13533–13544. https://doi.org/10.1021/acs.est.7b02695
Li Z, Xu S, Xiao G, Qian L, Song Y (2019) Removal of hexavalent chromium from groundwater using sodium alginate dispersed nano zero-valent iron. J Environ Manag 244:33–39. https://doi.org/10.1016/j.jenvman.2019.04.130
Li T, He Y, Peng X (2020) Efficient removal of tetrabromobisphenol A (TBBPA) using sewage sludge-derived biochar: adsorptive effect and mechanism. Chemosphere 251:126370. https://doi.org/10.1016/j.chemosphere2020.126370
Li D, Zhong Y, Wang H, Huang W, Peng P (2021a) Remarkable promotion in particle dispersion and electron transfer capacity of sulfidated nano zerovalent iron by coating alginate polymer. Sci Total Environ 759:143481. https://doi.org/10.1016/j.scitotenv.2020.143481
Li H, Si R, Wang W, Huang Y, Xiang M, Wang C, Chen S, Cao W, Lu Z, Huang M (2021b) Sulfidated nanoscale zero-valent iron dispersed in dendritic mesoporous silica nanospheres for degrading tetrabromobisphenol A. Colloids Surf A Physicochem Eng Asp 621:126586. https://doi.org/10.1016/j.colsurfa.2021.126586
Li J, Guo N, Zhao S, Xu J, Wang Y (2021c) Mechanisms of metabolic performance enhancement and ARGs attenuation during nZVI-assisted anaerobic chloramphenicol wastewater treatment. J Hazard Mater 419:126508. https://doi.org/10.1016/j.jhazmat.2021.126508
Li R, Li Q, Zhang W, Sun X, Li J, Shen J, Han W (2021d) Low dose of sulfur-modified zero-valent iron for decontamination of trace Cd(II)-complexes in high-salinity wastewater. Sci Total Environ 793:148579. https://doi.org/10.1016/j.scitotenv.2021.148579
Li Y, Deng M, Wang X, Wang Y, Li J, Xia S, Zhao J (2021e) In-situ remediation of oxytetracycline and Cr(VI) co-contaminated soil and groundwater by using blast furnace slag-supported nanosized Fe0/FeSx. Chem Eng J 412:128706. https://doi.org/10.1016/j.cej.2021.128706
Li M, Wei D, Zhang Z, Fan D, Du B, Zeng H, Li D, Zhang J (2022a) Enhancing 2,6-dichlorophenol degradation and nitrate removal in the nano-zero-valent iron (nZVI) solid-phase denitrification system. Chemosphere 287:132249. https://doi.org/10.1016/j.chemosphere.2021.132249
Li S, Wu Y, Zheng H, Li H, Zheng Y, Nan J, Ma J, Nagarajan D, Chang J (2022b) Antibiotics degradation by advanced oxidation process (AOPs): recent advances in ecotoxicity and antibiotic-resistance genes induction of degradation products. Chemosphere 311:136977. https://doi.org/10.1016/j.chemosphere.2022.136977
Liang L, Li X, Lin Z, Tian C, Guo Y (2020) The removal of Cd by sulfidated nanoscale zero-valent iron: the structural, chemical bonding evolution and the reaction kinetics. Chem Eng J 382:122933. https://doi.org/10.1016/j.cej.2019.122933
Liang L, Li W, Li Y, Zhou W, Chen J (2021) Removal of EDTA-chelated CdII by sulfidated nanoscale zero-valent iron: removal mechanisms and influencing factors. Sep Purif Technol 276:119332. https://doi.org/10.1016/j.seppur.2021.119332
Liao X, Zhang C, Wang Y, Tang M (2017) The abiotic degradation of methyl parathion in anoxic sulfur-containing system mediated by natural organic matter. Chemosphere 176:288–295. https://doi.org/10.1016/j.chemosphere.2017.02.109
Liu X, Cao Z, Yuan Z, Zhang J, Guo X, Yang Y, He F, Zhao Y, Xu J (2018) Insight into the kinetics and mechanism of removal of aqueous chlorinated nitroaromatic antibiotic chloramphenicol by nanoscale zero-valent iron. Chem Eng J 334:508–518. https://doi.org/10.1016/j.cej.2017.10.060
Liu J, Jiang J, Meng Y, Aihemaiti A, Xu Y, Xiang H, Gao Y, Chen X (2020a) Preparation, environmental application and prospect of biochar-supported metal nanoparticles: a review. J Hazard Mater 388:122026. https://doi.org/10.1016/j.jhazmat.2020.122026
Liu S, Feng H, Tang L, Dong H, Wang J, Yu J, Feng C, Liu Y, Luo T, Ni T (2020b) Removal of Sb(III) by sulfidated nanoscale zerovalent iron: the mechanism and impact of environmental conditions. Sci Total Environ 736:139629. https://doi.org/10.1016/j.scitotenv.2020.139629
Liu N, Gong Y, Peng X, Li S, Zhang W (2022a) A win-win solution to chromate removal by sulfidated nanoscale zero-valent iron in

sludge. J Hazard Mater 432:128683. https://doi.org/10.1016/j.jhazmat.2022.128683

Liu Y, Gao J, Wang Y, Duan W, Liu J, Zhang Y, Zhang H, Zhao M (2022b) The removal of antibiotic resistant bacteria and genes and inhibition of the horizontal gene transfer by contrastive research on sulfidated nanoscale zerovalent iron activating peroxymonosulfate or peroxydisulfate. J Hazard Mater 423:126866. https://doi.org/10.1016/j.jhazmat.2021.126866

Liu Y, Gao J, Wang Y, Duan W, Zhang Y, Zhang H, Zhao M (2022c) Synergistic effect of sulfidated nanoscale zerovalent iron in donor and recipient bacterial inactivation and gene conjugative transfer inhibition. J Hazard Mater 432:128722. https://doi.org/10.1016/j.jhazmat.2022.128722

Lv D, Zhou X, Zhou J, Liu Y, Li Y, Yang K, Lou Z, Baig SA, Wu D, Xu X (2018) Design and characterization of sulfide-modified nanoscale zerovalent iron for cadmium(II) removal from aqueous solutions. Appl Surf Sci 442:114–123. https://doi.org/10.1016/j.apsusc.2018.02.085

Lv D, Zhou J, Cao Z, Xu J, Liu Y, Li Y, Yang K, Lou Z, Lou L, Xu X (2019) Mechanism and influence factors of chromium(VI) removal by sulfide-modified nanoscale zerovalent iron. Chemosphere 224:306–315. https://doi.org/10.1016/j.chemosphere.2019.02.109

Ma D, Yi H, Lai C, Liu X, Huo X, An Z, Li L, Fu Y, Li B, Zhang M, Qin L, Liu S, Yang L (2021) Critical review of advanced oxidation processes in organic wastewater treatment. Chemosphere 275:130104. https://doi.org/10.1016/j.chemosphere.2021.130104

Macêdo WV, Poulsen JS, Oliveira GHD, Nielsen JL, Zaiat M (2022) Tetrabromobisphenol A (TBBPA) biodegradation in acidogenic systems: one step further on where and who. Sci Total Environ 808:152016. https://doi.org/10.1016/j.scitotenv.2021.152016

Mangayayam M, Dideriksen K, Ceccato M, Tobler DJ (2019) The structure of sulfidized zero-valent iron by one-pot synthesis: impact on contaminant selectivity and long-term performance. Environ Sci Technol 53:4389–4396. https://doi.org/10.1021/acs.est.8b06480

Okeke ES, Huang B, Mao G, Chen Y, Zeng Z, Qian X, Wu X, Feng W (2022) Review of the environmental occurrence, analytical techniques, degradation and toxicity of TBBPA and its derivatives. Environ Res 206:112594. https://doi.org/10.1016/j.envres.2021.112594

Pang H, Diao Z, Wang X, Ma Y, Yu S, Zhu H, Chen Z, Hu B, Chen J, Wang X (2019) Adsorptive and reductive removal of U(VI) by Dictyophora indusiate-derived biochar supported sulfide NZVI from wastewater. Chem Eng J 366:368–377. https://doi.org/10.1016/j.cej.2019.02.098

Qin L, Wang L, Sun X, Yu L, Wang M, Chen S (2022) Ecological toxicity (ECx) of Pb and its prediction models in Chinese soils with different physiochemical properties. Sci Total Environ 853:158769. https://doi.org/10.1016/j.scitotenv.2022.158769

Qu J, Liu Y, Cheng L, Jiang Z, Zhang G, Deng F, Wang L, Han W, Zhang Y (2021) Green synthesis of hydrophilic activated carbon supported sulfide nZVI for enhanced Pb(II) scavenging from water: characterization, kinetics, isotherms and mechanisms. J Hazard Mater 403:123607. https://doi.org/10.1016/j.jhazmat.2020.123607

Rajajayavel SRC, Ghoshal S (2015) Enhanced reductive dechlorination of trichloroethylene by sulfidated nanoscale zerovalent iron. Water Res 78:144–153. https://doi.org/10.1016/j.watres.2015.04.009

Semerád J, Filip J, Ševců A, Brumovský M, Nguyen NHA, Mikšíček J, Lederer T, Filipová A, Boháčková J, Cajthaml T (2020) Environmental fate of sulfidated nZVI particles: the interplay of nanoparticle corrosion and toxicity during aging. Environ Sci Nano 7:1794–1806. https://doi.org/10.1039/d0en00075b

Shen W, Xu J, Zhu L (2021) Triton X-100 improves the reactivity and selectivity of sulfidized nanoscale zerovalent iron toward tetrabromobisphenol A: implications for groundwater and soil remediation. J Hazard Mater 416:126119. https://doi.org/10.1016/j.jhazmat.2021.126119

Singh P, Pal P, Mondal P, Saravanan G, Nagababu P, Majumdar S, Labhsetwar N, Bhowmick S (2021) Kinetics and mechanism of arsenic removal using sulfide-modified nanoscale zerovalent iron. Chem Eng J 412:128667. https://doi.org/10.1016/j.cej.2021.128667

Song S, Su Y, Adeleye AS, Zhang Y, Zhou X (2017) Optimal design and characterization of sulfide-modified nanoscale zerovalent iron for diclofenac removal. Appl Catal B Environ 201:211–220. https://doi.org/10.1016/j.apcatb.2016.07.055

Song X, Ni J, Liu D, Shi W, Yuan Y, Cui F, Tian J, Wang W (2022) Molybdenum disulfide as excellent Co-catalyst boosting catalytic degradation of sulfamethoxazole by nZVI/PDS process. Sep Purif Technol 285:120398. https://doi.org/10.1016/j.seppur.2021.120398

Song H, Liang W, Luo K, Wang G, Li Q, Ji X, Wan J, Shao X, Gong K, Zhang W, Peng C (2023) Simultaneous stabilization of Pb, Cd, and As in soil by rhamnolipid coated sulfidated nano zerovalent iron: effects and mechanisms. J Hazard Mater 443:130259. https://doi.org/10.1016/j.jhazmat.2022.130259

Sredlova K, Cajthaml T (2021) Recent advances in PCB removal from historically contaminated environmental matrices. Chemosphere 287:132096. https://doi.org/10.1016/j.chemosphere.2021.132096

Su Y, Adeleye AS, Keller AA, Huang Y, Dai C, Zhou X, Zhang Y (2015) Magnetic sulfide-modified nanoscale zerovalent iron (S-nZVI) for dissolved metal ion removal. Water Res 74:47–57. https://doi.org/10.1016/j.watres.2015.02.004

Su Y, Jassby D, Song S, Zhou X, Zhao H, Filip J, Petala E, Zhang Y (2018) Enhanced oxidative and adsorptive removal of diclofenac in heterogeneous fenton-like reaction with sulfide modified nanoscale zerovalent iron. Environ Sci Technol 52:6466–6475. https://doi.org/10.1021/acs.est.8b00231

Su Y, Jassby D, Zhang Y, Keller AA, Adeleye AS (2020) Comparison of the colloidal stability, mobility, and performance of nanoscale zerovalent iron and sulfidated derivatives. J Hazard Mater 396:122691. https://doi.org/10.1016/j.jhazmat.2020.122691

Sun Y, Gu M, Lyu S, Brusseau ML, Li M, Lyu Y, Xue Y, Qiu Z, Sui Q (2020) Efficient removal of trichloroethene in oxidative environment by anchoring nano FeS on reduced graphene oxide supported nZVI catalyst: the role of FeS on oxidant decomposition and iron leakage. J Hazard Mater 392:122328. https://doi.org/10.1016/j.jhazmat.2020.122328

Tan X, Deng Y, Shu Z, Zhang C, Ye S, Chen Q, Yang H, Yang L (2022) Phytoremediation plants (ramie) and steel smelting wastes for calcium silicate coated-nZVI/biochar production: environmental risk assessment and efficient As(V) removal mechanisms. Sci Total Environ 844:156924. https://doi.org/10.1016/j.scitotenv.2022.156924

Tang J, Tang L, Feng H, Zeng G, Dong H, Zhang C, Huang B, Deng Y, Wang J, Zhou Y (2016) pH-dependent degradation of p-nitrophenol by sulfidated nanoscale zerovalent iron under aerobic or anoxic conditions. J Hazard Mater 320:581–590. https://doi.org/10.1016/j.jhazmat.2016.07.042

Uddin MK (2017) A review on the adsorption of heavy metals by clay minerals, with special focus on the past decade. Chem Eng J 308:438–462. https://doi.org/10.1016/j.cej.2016.09.029

Wang N, Wang A, Kong L, He M (2018) Calculation and application of Sb toxicity coefficient for potential ecological risk assessment. Sci Total Environ 610–611:167–174. https://doi.org/10.1016/j.scitotenv.2017.07.268

Wang B, Dong H, Li L, Wang Y, Ning Q, Tang L, Zeng G (2020a) Influence of different co-contaminants on trichloroethylene

removal by sulfide-modified nanoscale zero-valent iron. Chem Eng J 381:122773. https://doi.org/10.1016/j.cej.2019.122773

Wang Y, Gao J, Duan W, Zhang W, Zhao Y, Liu J (2020b) Inactivation of sulfonamide antibiotic resistant bacteria and control of intracellular antibiotic resistance transmission risk by sulfide-modified nanoscale zero-valent iron. J Hazard Mater 400:123226. https://doi.org/10.1016/j.jhazmat.2020.123226

Wang H, Zhong Y, Zhu X, Li D, Deng Y, Huang W, Peng P (2021) Enhanced tetrabromobisphenol A debromination by nanoscale zero valent iron particles sulfidated with S(0) dissolved in ethanol. Environ Sci Process Impacts 23:86–97. https://doi.org/10.1039/d0em00375a

Wang J, Xu S, Zhao K, Song G, Zhao S, Liu R (2023) Risk control of antibiotics, antibiotic resistance genes (ARGs) and antibiotic resistant bacteria (ARB) during sewage sludge treatment and disposal: a review. Sci Total Environ 877:162772. https://doi.org/10.1016/j.scitotenv.2023.162772

Wei A, Ma J, Chen J, Zhang Y, Song J, Yu X (2018) Enhanced nitrate removal and high selectivity towards dinitrogen for groundwater remediation using biochar-supported nano zero-valent iron. Chem Eng J 353:595–605. https://doi.org/10.1016/j.cej.2018.07.127

Wu D, Peng S, Yan K, Shao B, Feng Y, Zhang Y (2018) Enhanced As(III) sequestration using sulfide-modified nano-scale zero-valent iron with a characteristic core–shell structure: sulfidation and As distribution. ACS Sustain Chem Eng 6:3039–3048. https://doi.org/10.1021/acssuschemeng.7b02787

Wu J, Zhao J, Hou J, Zeng R, Xing B (2019) Degradation of tetrabromobisphenol A by sulfidated nanoscale zerovalent iron in a dynamic two-step anoxic/oxic process. Environ Sci Technol 53:8105–8114. https://doi.org/10.1021/acs.est.8b06834

Wu W, Han L, Nie X, Gu M, Li J, Chen M (2021) Effects of multiple injections on the transport of CMC-nZVI in saturated sand columns. Sci Total Environ 784:147160. https://doi.org/10.1016/j.scitotenv.2021.147160

Wu G, Kong W, Gao Y, Kong Y, Dai Z, Dan H, Shang Y, Wang S, Yin F, Yue Q, Gao B (2022a) Removal of chloramphenicol by sulfide-modified nanoscale zero-valent iron activated persulfate: performance, salt resistance, and reaction mechanisms. Chemosphere 286:131876. https://doi.org/10.1016/j.chemosphere.2021.131876

Wu L, Lin Q, Fu H, Luo H, Zhong Q, Li J, Chen Y (2022b) Role of sulfide-modified nanoscale zero-valent iron on carbon nanotubes in nonradical activation of peroxydisulfate. J Hazard Mater 422:126949. https://doi.org/10.1016/j.jhazmat.2021.126949

Xiao S, Jin Z, Dong H, Xiao J, Li Y, Li L, Li R, Chen J, Tian R, Xie Q (2022) A comparative study on the physicochemical properties, reactivity and long-term performance of sulfidized nanoscale zerovalent iron synthesized with different kinds of sulfur precursors and procedures in simulated groundwater. Water Res 212:118097. https://doi.org/10.1016/j.watres.2022.118097

Xu J, Cao Z, Wang Y, Zhang Y, Gao X, Ahmed MB, Zhang J, Yang Y, Zhou J, Lowry GV (2019a) Distributing sulfidized nanoscale zerovalent iron onto phosphorus-functionalized biochar for enhanced removal of antibiotic florfenicol. Chem Eng J 359:713–722. https://doi.org/10.1016/j.cej.2018.11.180

Xu J, Cao Z, Zhou H, Lou Z, Wang Y, Xu X, Lowry GV (2019b) Sulfur dose and sulfidation time affect reactivity and selectivity of post-sulfidized nanoscale zerovalent iron. Environ Sci Technol 53:13344–13352. https://doi.org/10.1021/acs.est.9b04210

Xu J, Wang Y, Weng C, Bai W, Jiao Y, Kaegi R, Lowry GV (2019c) Reactivity, selectivity, and long-term performance of sulfidized nanoscale zerovalent iron with different properties. Environ Sci Technol 53:5936–5945. https://doi.org/10.1021/acs.est.9b00511

Xu B, Li D, Qian T, Jiang H (2020a) Boosting the activity and environmental stability of nanoscale zero-valent iron by montmorillonite supporting and sulfidation treatment. Chem Eng J 387:124063. https://doi.org/10.1016/j.cej.2020.124063

Xu J, Avellan A, Li H, Clark EA, Henkelman G, Kaegi R, Lowry GV (2020b) Iron and sulfur precursors affect crystalline structure, speciation, and reactivity of sulfidized nanoscale zerovalent iron. Environ Sci Technol 54:13294–13303. https://doi.org/10.1021/acs.est.0c03879

Xu J, Avellan A, Li H, Liu X, Noël V, Lou Z, Wang Y, Kaegi R, Henkelman G, Lowry GV (2020c) Sulfur loading and speciation control the hydrophobicity, electron transfer, reactivity, and selectivity of sulfidized nanoscale zerovalent iron. Adv Mater 32:1906910. https://doi.org/10.1002/adma.201906910

Xu W, Hu X, Lou Y, Jiang X, Shi K, Tong Y, Xu X, Shen C, Hu B, Lou L (2020d) Effects of environmental factors on the removal of heavy metals by sulfide-modified nanoscale zerovalent iron. Environ Res 187:109662. https://doi.org/10.1016/j.envres.2020.109662

Xu W, Li Z, Shi S, Qi J, Cai S, Yu Y, O'Carroll DM, He F (2020e) Carboxymethyl cellulose stabilized and sulfidated nanoscale zerovalent iron: characterization and trichloroethene dechlorination. Appl Catal B Environ 262:118303. https://doi.org/10.1016/j.apcatb.2019.118303

Xu B, Qian T, Chen S, Yang J, Jiang H (2021) Preparation of highly stable and easily regenerated sulfuretted nZVI via one-pot fast pyrolysis method for the removal of diclofenac. J Environ Chem Eng 9:105425. https://doi.org/10.1016/j.jece.2021.105425

Xu H, Li X, Gao M, Hu X, Zhang X, Li Y, Xu X, Hu J, Tang C, Hu X (2022) Chitosan and biochar synergize the efficient elimination of lead from wastewater by sulfidised nano-zero-valent iron. J Environ Chem Eng 10:107101. https://doi.org/10.1016/j.jece.2021.107101

Yan J, Han L, Gao W, Xue S, Chen M (2015) Biochar supported nanoscale zerovalent iron composite used as persulfate activator for removing trichloroethylene. Bioresour Technol 175:269–274. https://doi.org/10.1016/j.biortech.2014.10.103

Ye S, Tan X, Yang H, Xiong J, Zhu H, Song H, Chen G (2022) Catalytic removal of attached tetrabromobisphenol A from microplastic surface by biochar activating oxidation and its impact on potential of disinfection by-products formation. Water Res 225:119191. https://doi.org/10.1016/j.watres.2022.119191

Yoon H, Pangging M, Jang M, Hwang Y, Chang Y (2018) Impact of surface modification on the toxicity of zerovalent iron nanoparticles in aquatic and terrestrial organisms. Ecotoxicol Environ Saf 163:436–443. https://doi.org/10.1016/j.ecoenv.2018.07.099

Yu Q, Guo J, Muhammad Y, Li Q, Lu Z, Yun J, Liang Y (2020) Mechanisms of enhanced hexavalent chromium removal from groundwater by sodium carboxymethyl cellulose stabilized zerovalent iron nanoparticles. J Environ Manag 276:111245. https://doi.org/10.1016/j.jenvman.2020.111245

Yu Z, Rabiee H, Guo J (2021) Synergistic effect of sulfidated nano zerovalent iron and persulfate on inactivating antibiotic resistant bacteria and antibiotic resistance genes. Water Res 198:117141. https://doi.org/10.1016/j.watres.2021.117141

Yu X, Jin X, Li M, Yu Y, Zhu M, Tang S, Zhou H, Wang K, Dou R, Sun J (2022a) Degradation mechanism of tetracycline using sulfidated nanoscale zerovalent iron driven peroxymonosulfate and metabolomic insights into environmental risk of intermediates products. Chem Eng J 430:133141. https://doi.org/10.1016/j.cej.2021.133141

Yu X, Jin X, Wang N, Yu Y, Zhu X, Chen M, Zhong Y, Sun J, Zhu L (2022b) Transformation of sulfamethoxazole by sulfidated nanoscale zerovalent iron activated persulfate: mechanism and risk assessment using environmental metabolomics. J Hazard Mater 428:128244. https://doi.org/10.1016/j.jhazmat.2022.128244

Yuan X, Li T, He Y, Xue N (2021) Degradation of TBBPA by nZVI activated persulfate in soil systems. Chemosphere 284:131166. https://doi.org/10.1016/j.chemosphere.2021.131166

Zeng S, Zhong D, Xu Y, Zhong N (2022) A novel sulfide-modified nanoscale zero valent iron supported on porous anion exchange resin composite for Cr(VI) effective removal from waste. Chem Phys Lett 794:139494. https://doi.org/10.1016/j.cplett.2022.139494

Zhang D, Li Y, Tong S, Jiang X, Wang L, Sun X, Li J, Liu X, Shen J (2018) Biochar supported sulfide-modified nanoscale zero-valent iron for the reduction of nitrobenzene. RSC Adv 8:22161–22168. https://doi.org/10.1039/c8ra04314k

Zhang D, Li Y, Sun A, Tong S, Su G, Jiang X, Li J, Han W, Sun X, Wang L, Shen J (2019a) Enhanced nitrobenzene reduction by modified biochar supported sulfidated nano zerovalent iron: comparison of surface modification methods. Sci Total Environ 694:133701. https://doi.org/10.1016/j.scitotenv.2019.133701

Zhang D, Shen J, Shi H, Su G, Jiang X, Li J, Liu X, Mu Y, Wang L (2019b) Substantially enhanced anaerobic reduction of nitrobenzene by biochar stabilized sulfide-modified nanoscale zero-valent iron: process and mechanisms. Environ Int 131:105020. https://doi.org/10.1016/j.envint.2019.105020

Zhang C, Lu J, Wu J (2020a) One-step green preparation of magnetic seaweed biochar/sulfidated Fe(0) composite with strengthen adsorptive removal of tetrabromobisphenol A through in situ reduction. Bioresour Technol 307:123170. https://doi.org/10.1016/j.biortech.2020.123170

Zhang D, Li Y, Sun A, Tong S, Jiang X, Mu Y, Li J, Han W, Sun X, Wang L, Shen J (2020b) Optimization of S/Fe ratio for enhanced nitrobenzene biological removal in anaerobic system amended with sulfide-modified nanoscale zerovalent iron. Chemosphere 247:125832. https://doi.org/10.1016/j.chemosphere.2020.125832

Zhang M, Yi K, Zhang X, Han P, Liu W, Tong M (2020c) Modification of zero valent iron nanoparticles by sodium alginate and bentonite: enhanced transport, effective hexavalent chromium removal and reduced bacterial toxicity. J Hazard Mater 388:121822. https://doi.org/10.1016/j.jhazmat.2019.121822

Zhang W, Gao J, Duan W, Zhang D, Jia J, Wang Y (2020d) Sulfidated nanoscale zero-valent iron is an efficient material for the removal and regrowth inhibition of antibiotic resistance genes. Environ Pollut 263:114508. https://doi.org/10.1016/j.envpol.2020.114508

Zhang J, Yu H, Xu W, Shi H, Hu X, Xu J, Lou L (2023) Adsorption-reduction coupling mechanism and reductive species during efficient florfenicol removal by modified biochar supported sulfidized nanoscale zerovalent iron. Environ Res 216:114782. https://doi.org/10.1016/j.envres.2022.114782

Zhao X, Liu W, Cai Z, Han B, Qian T, Zhao D (2016) An overview of preparation and applications of stabilized zero-valent iron nanoparticles for soil and groundwater remediation. Water Res 100:245–266. https://doi.org/10.1016/j.watres.2016.05.019

Zhao L, Zhao Y, Yang B, Teng H (2019) Application of carboxymethyl cellulose–stabilized sulfidated nano zerovalent iron for removal of Cr(VI) in simulated groundwater. Water Air Soil Pollut 230:113. https://doi.org/10.1007/s11270-019-4166-1

Zhao G, Zou J, Chen X, Liu L, Wang Y, Zhou S, Long X, Yu J, Jiao F (2021a) Iron-based catalysts for persulfate-based advanced oxidation process: microstructure, property and tailoring. Chem Eng J 421:127845. https://doi.org/10.1016/j.cej.2020.127845

Zhao J, Su A, Tian P, Tang X, Collins RN, He F (2021b) Arsenic (III) removal by mechanochemically sulfidated microscale zero valent iron under anoxic and oxic conditions. Water Res 198:117132. https://doi.org/10.1016/j.watres.2021.117132

Zhou C, Han C, Min X, Yang T (2021a) Enhancing arsenic removal from acidic wastewater using zeolite-supported sulfide nanoscale zero-valent iron: the role of sulfur and copper. J Chem Technol Biotechnol 96:2042–2052. https://doi.org/10.1002/jctb.6734

Zhou C, Han C, Min X, Yang T (2021b) Simultaneous adsorption of As(V) and Cr(VI) by zeolite supporting sulfide nanoscale zero-valent iron: competitive reaction, affinity and removal mechanism. J Mol Liq 338:116619. https://doi.org/10.1016/j.molliq.2021116619

Zhou C, Han C, Min X, Yang T (2022) Effect of different sulfur precursors on efficient chromium(VI) removal by ZSM-5 zeolite supporting sulfide nano zero-valent iron. Chem Eng J 427:131515. https://doi.org/10.1016/j.cej.2021.131515

Zhu S, Ho S, Huang X, Wang D, Yang F, Wang L, Wang C, Cao X, Ma F (2017) Magnetic nanoscale zerovalent iron assisted biochar: interfacial chemical behaviors and heavy metals remediation performance. ACS Sustain Chem Eng 5:9673–9682. https://doi.org/10.1021/acssuschemeng.7b00542

Zhu X, Le T, Du J, Xu T, Cui Y, Ling H, Kim S (2021) Novel core-shell sulfidated nano-Fe(0) particles for chromate sequestration: promoted electron transfer and Fe(II) production. Chemosphere 284:131379. https://doi.org/10.1016/j.chemosphere.2021.131379

Zhuang M, Achmon Y, Cao Y, Liang X, Chen L, Wang H, Siame BA, Leung KY (2021a) Distribution of antibiotic resistance genes in the environment. Environ Pollut 285:117402. https://doi.org/10.1016/j.envpol.2021.117402

Zhuang M, Wang H, Qi L, Cui L, Quan G, Yan J (2021b) Production of activated biochar via a self-blowing strategy-supported sulfidated nanoscale zerovalent iron with enhanced reactivity and stability for Cr(VI) reduction. J Clean Prod 315:128108. https://doi.org/10.1016/j.jclepro.2021.128108